Physics – Uspekhi **51** (1) 57 – 77 (2008)

REVIEWS OF TOPICAL PROBLEMS

PACS numbers: **41.50. + h**, **87.59. – e**, 87.64.Bx

Recent advances in X-ray refractive optics

V V Aristov, L G Shabel'nikov

DOI: 10.1070/PU2008v051n01ABEH006431

Contents

Abstract. X-ray refractive optics has made rapid strides to a large degree due to the work of Russian scientists, and has now become one of the most rapidly advancing areas in modern physical optics. This review outlines the results of investigation of refractive devices and analysis of their properties. The conception of planar lenses made of silicon and other materials is set forth. We discuss the applications of refractive lenses to the transformation of X-ray images, photonic crystal research, and the development of focusing devices in high-energy X-ray telescopes.

1. Introduction

In a very wide electromagnetic radiation spectrum, the X-ray wavelength range is of considerable interest. In the initial stage of mastering X-ray radiation [1], use was made of shadow microscopy, photoelectron spectroscopy, and diffraction phenomena in crystals. Recent decades have seen an increasingly rapid advancement in X-ray optics which invokes the notions and theoretical apparatus of the classical optics of visible light [2]. The inclusion of the peculiarities of interaction of short-wave radiation with matter [3] leads to X-ray optical analogs which are atypical with regard to conventional optics and do not reduce to simple scaling according to the wavelength ratio [4]. In this case, it is required to elaborate the theoretical description of X-ray optical elements and systems, as well as their fabrication methods and technologies.

The problem of developing devices for controlling X-ray radiation emerged with the discovery of X-rays [1]. Following the discovery of X-ray diffraction by crystals [5] and experiments in the reflection of X-rays from smooth surfaces [3, 6], which revealed the electromagnetic nature of these rays, a start was made on investigations aimed at creating their optical analogs, which are reviewed in Ref. [4].

X-ray radiation, which had long been considered as an instrument for studying the atomic crystalline structure and for monitoring the perfection of crystals, found wide application in medicine. In this case, collimators and monochromators of different kinds were mainly the elements of X-ray optics, while reflective profiled mirrors and curved crystals had fewer uses. In the 1970s, the feasibilities of the technological application of this kind of electromagnetic

V V Aristov, L G Shabel'nikov Institute for Microelectronics Technology and High Purity Materials, Russian Academy of Sciences,
142432 Chernogolovka, Moscow region, Russian Federation
Tel. (7-495) 962 80 71, (7-496) 524 40 81
E-mail: aristov@ipmt-hpm.ac.ru, lgs@ipmt-hpm.ac.ru

Received 23 July 2007
Uspekhi Fizicheskikh Nauk **178** (1) 61 – 83 (2008)
DOI: 10.3367/UFNr.0178.200801c.0061
Translated by E N Ragozin; edited by A Radzig

radiation for producing nanostructures with a resolution of 5–10 nm by X-ray lithographic techniques [7] were demonstrated. A demand for the development of X-ray lithography and a set of local techniques of X-ray analysis for a wide circle of practical implementations related primarily to the development of microelectronics fostered the advancement of both X-ray optics and specialized electron accelerators intended for the generation of radiation with unique properties — synchrotron radiation (SR). Information about the properties of SR, the key parameters of synchrotrons, and the geography of their distribution throughout the world may be found, for instance, in Ref. [8]. At present there exist third-generation SR sources, and so-called fourth-generation synchrotrons and free-electron lasers are at the stage of development or experimental mastering [9]. It is valid to say that the vast X-ray radiation range, which is adjacent to the vacuum ultraviolet range at photon energies of the order of 100 eV, and borders on the range of γ-ray radiation of radioactive nuclei at energies of 100 keV and above, is becoming progressively more accessible. Research in different areas has become possible due to SR sources and the wide use of focusing elements capable of affording a high spatial resolution in the formation of X-ray beams and X-ray image transmission. In a number of cases, X-ray optical elements make it possible to ensure conditions for realizing the above methods by way of concentrating and focusing the radiation. Furthermore, the demand for mastering a very wide short-wave radiation range to a large extent lent impetus to the development and broadening of the component basis of X-ray optics in close correlation with the possibilities furnished by microelectronic technologies. Recently, reports have appeared about the fabrication of X-ray optical devices by means of nanotechnologies as well.

The development of X-ray optical devices basically relies on harnessing the diffraction effects and the inclusion of the properties of interaction between an electromagnetic wave belonging to this range and matter. This underlies the division of focusing X-ray optical devices into the following classes (or types) accepted in the literature:

— **reflective optics**, which comprises specular optical elements reliant on total external reflection [10] and multiple reflections [11]. Also among these are multilayer interference mirrors [12]. Here, mention should first of all be made of short-period mirrors which possess a broadened spectral range [13], as well as of multilayer coatings on special aspherically shaped substrates [14] for beam formation and image transmission systems;

— **diffraction optics**, which comprises transmission Fresnel zone plates [12], Bragg–Fresnel elements based on multilayer mirrors and perfect crystals [15, 16], diffraction grazing-incidence lenses [17], and synthetic X-ray holograms [18];

— **X-ray refractive optics**, which is represented by compound refractive lenses [19–22], focusing elements based on kinoform refractive profiles [23–28], and elements made up of prism sets [29–31];

— **X-ray waveguides** based on thin-film structures [16, 32, 33], including resonator waveguides [34], waveguides with an air gap [35, 36], and two-dimensional waveguides [37].

The majority of the X-ray optical elements listed above have analogs among conventional optical devices for the visible range. Among these are specular optical elements, Fresnel zone plates, and waveguides, as well as elements reliant on the refraction effect.

Among the unconventional devices are primarily Bragg–Fresnel optical elements, wherein the effect of Bragg diffraction by the crystal structure is combined with the diffraction by a specially made Fresnel zone structure. Also noteworthy is the fact that in the Bragg diffraction recorded in the near Fresnel zone it is possible to observe the effect of angular dispersion of the refractive index, with consequential radiation focusing into a plane-parallel crystal [38, 39]. Also among the unconventional devices are the elements of multiplicative kinoform optics which is ineffective and hardly used in the visible region. In the X-ray band, this area of research [23–28] is in progressively increasing demand, which explains its more detailed discussion in subsequent sections of our review.

The creation of refractive lenses and prisms, which are direct and immediate analogs of devices working in the visible range, had long been thought of as being impossible because of the extremely small deviation of the refractive index from unity, and such X-ray optics had been the subject of theoretical reasoning and estimates (see the references cited in Refs [12, 40]). The advent of compound refractive lenses [19], which attracted considerable attention of researchers throughout the world, significantly broadened both the possibilities for making X-ray optical devices and the spectral range of their applications.

In recent years, refractive optics has turned into a branch of X-ray optics in its own right, which has seen the realization of novel and uncommon approaches to lens development, pertaining to both design solutions and fabrication technologies. Several important scientific results of general physical significance have been obtained with the aid of compound refractive lenses [41, 42]. It should be particularly emphasized that the advancement of X-ray refractive optics takes place against the background of sustained efforts of researchers to achieve radiation focusing in the nanometer wave range [32, 37, 43, 44]. New approaches have been formulated [45] and their elaboration would allow bringing the spatial resolution to magnitudes characteristic of modern techniques of scanning microscopy.

The advent of new-generation X-ray focusers brings about a substantial broadening of the potentialities of well-known techniques and enables the application of approaches and methods that would make it possible to gain new structural information in close correlation with the physical characteristics of a large number of objects. In this respect, the promise of X-ray refractive optics is considerable. The limited volume of this paper and the existence of a wealth of evidence on all types of the X-ray optical elements was an additional reason to single out only the elements stated in the title of our review.

2. Basic notions of X-ray refractive optics

2.1 Refractive profiles of X-ray lenses

In the foregoing we mentioned the seemingly fundamental difficulty in developing lenses, which are quite commonplace in the visible region, for the X-ray range — the small deviation of the refractive index from unity ($\delta = 1 - n \approx 10^{-5} - 10^{-6}$), and a relatively high radiation absorption [12]. A comparison of the parameters given below shows that only a relatively small set of materials wherein refraction prevails over absorption (chemical elements, inorganic and organic compounds with $Z_{\rm eff} \leqslant 12-14$) are suited for the implementation of refractive optical elements. When use is made of these materials, owing to the extremely low magnitude of the refractive index decrement it is required to form refractive profiles with radii of curvature of the order of several micrometers.

Let us consider the refractive profile shape required to focus rays on a point lying on the optical axis. It is pertinent to note that this formulation is typical for the majority of problems solved by means of X-ray optical devices for a small-sized remote source. The profile shape can be explicitly defined in the form of a piecewise-smooth and single-valued function $Y(x)$. Such a profile, which satisfies the condition of equal optical paths for points equidistant from the optical axis, is described by an even function $Y(x) = Y(-x)$.

To the refractive profile of biprisms [29] there corresponds a dependence $Y_1(x) \approx |x|$ considered in Section 6. A composition of rectilinear segments defining a saw-tooth profile $Y(x)$ also affords radiation focusing [46]. Multiprism elements described in Refs [30, 31] also possess this profile.

The focusing of a plane monochromatic wave into a refractive profile may be considered with ease in the model of Ref. [47], which takes into account only the changes in the transmitted radiation phase, similarly to that with a Fresnel phase zone plate [12, 15, 16]. The change of wave-vector directions in individual portions of the transmitted wave is assumed to be negligible owing to the smallness of the refractive index decrement. Then, the refractive profile is equivalent to a thin lens. Under the above limitations, it would suffice to derive the profile equation in the case of wave incidence onto the input surface of a focusing element, which is defined by a plane OP (Fig. 1). When a plane wave is incident on the input plane of a focusing element, according to the Huygens – Fresnel principle it is required to consider the secondary sources excited by the wave. When P' is the focal point, the optical path from the input plane P to point P' is equal for all sources located on the profile $AP' = OP'$ for an arbitrary point A. The inequality $\mathrm{Re}\, n = 1 - \delta < 1$ enables compensating for the optical path for an arbitrary point A. Then, according to Ref. [47], the perfect shape of refractive surfaces for X-ray lenses is close to the parabolic one in the approximation of paraxial optics (see Fig. 1):

$$Y(x) = \frac{x^2 L_\pi}{2F\lambda}\left[1 - \left(\frac{x}{2F}\right)^2\right]. \quad (1)$$

The relationship between the radius of curvature of the parabolic profile and its focal length in the form $R = 2F\delta$ also follows from formula (1).

The functions $Y(x)$, which are given in implicit form and are the solution of the equation $F\big[Y(x), x\big] = 0$, may also be involved in the search for the desired shape of a refractive

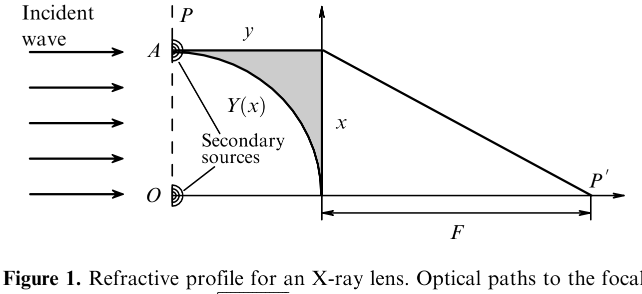

Figure 1. Refractive profile for an X-ray lens. Optical paths to the focal point are $AP' = yn + \sqrt{x^2 + F^2}$, and $OP' = y + F$, with $n = 1 - \delta + i\beta$, and $\mathrm{Re}\, n = 1 - \delta < 1$.

profile. Among the possible solutions, mention should first of all be made of equations of a circle [19 – 22] or an ellipse [27, 28]. For these two types, the lens has a limited aperture, unlike the parabolic profile (see Fig. 1). Then, according to the treatment performed, the circular and elliptical shapes are not optimal for X-ray lenses.

Therefore, a focal distance of 10 cm $\leqslant F \leqslant$ 1 m is attainable for a radius of curvature of a single refractive profile equal to 1 μm $\leqslant R \leqslant$ 10 μm for typical values of the refractive index decrement δ given above. Fabricating suchlike refractive profiles of X-ray lenses calls for the development of an adequate technology. Let us estimate the effect of technological errors in the fabrication of X-ray lenses that are associated with random departures of their refractive profile from a parabola, which gives rise to irregular phase interruptions in the transmitted wave. For a single lens with random profile distortions, the intensity $\langle I \rangle$ at the focal point is described by the expression [48]

$$\langle I \rangle = I \exp\left[-\left(\frac{\pi \Delta Y}{L_\pi}\right)^2\right]. \quad (2)$$

Here, I is the intensity at the focal point for a perfect profile.

Relation (2) coincides in form with the recording of the intensity of scattering from distorted crystals (thermal vibrations, displacements of atoms from their regular positions) in terms of the Debye – Waller factor [48]. Dependences similar to relationship (2) are known for the scattering of an X-ray wave by a surface with statistically distributed irregularities [11].

Another technological source of phase interruptions in the transmitted wave arises from the approximation of a parabola (see Fig. 1) by a set of rectilinear segments [49]. In this case, systematic phase interruptions emerge due to the difference between the wave optical paths in the parabolic and approximating profiles. In this case, to retain the coherence of the contributions from the wave transmitted through the portions of the approximating profile requires the fulfillment of the Rayleigh criterion which is written out in this instance as

$$\Delta\Phi = \frac{\pi l}{L_\pi} \leqslant \frac{\pi}{4}. \quad (3)$$

It may be shown [49] that the magnitude of l is equal for all profile partition segments, irrespective of the segment number. Then, it follows from criterion (3) that a limitation for the profile partition step $\varDelta$ may be expressed in the form

$$\varDelta \leqslant \sqrt{\frac{R\lambda}{\delta}} = \sqrt{F\lambda}. \quad (4)$$

Therefore, the partition step must not exceed the Fresnel radius for a given single lens.

Among the important characteristics of refractive optical elements is the integral transmittance T defined as [50, 51]

$$T = \frac{I}{I_0} = \frac{1}{A}\int_{-A/2}^{A/2} \exp\big[-\mu Y(x)\big]\,dx. \quad (5)$$

With the inclusion of absorption in the refractive profile, the total aperture reduces to the effective aperture $A_{\mathrm{eff}} = AT$ [19, 51] which specifies the intensity gain factor in the focal spot. It is noteworthy that the interaction of transmitted radiation with the refractive lens material gives rise to the emergence of the channels of intensity loss in the focal spot. Emphasis in this case should be put on small-angle scattering, as well as on scattering through a wider angular interval, depending on the structure peculiarities of the lens material. To these must be added the loss channels related to the imperfections of the refractive profile considered above.

In the general case, the technological errors in the formation of refractive profiles are responsible for the blurring of the caustic region where not only a loss in intensity but also the focal spot distortion show their worth. The above effects were considered with the help of techniques involving numerical calculations for a set of model profile distortions [47, 48, 52, 53].

It is pertinent to note that the precision of lens formation is determined by the quantity $\lambda/\pi(n-1)$, which lies in the range between several micrometers to tenths of a micrometer in the visible light optics. For a glass lens with $n = 1.5$ for $\lambda = 0.5$ μm, for instance, an accuracy of 0.3 μm may be considered sufficient. In the X-ray band, the admissible departures of the refractive profile under fabrication from the ideal one are substantially greater. In particular, typical values of the phase-shifting path for materials which may be employed in the fabrication of X-ray lenses amount to 10–100 μm. Therefore, the requirements on the accuracy of refractive profile fabrication are, in view of the possible departures ranging into the fractions of a micrometer, attainable for present-day technologies.

For comparison purposes we mention that the technological errors in reproducing total external reflection mirrors or Fresnel zone plates [12, 16, 43] range from a few to dozens of nanometers. It should be emphasized that in several cases this accuracy is achieved in the fabrication of aspherical surfaces of the optical elements for projection X-ray lithography, the fabrication being based on proprietary technologies and testing methods [54].

2.2 X-ray lens materials

The wave absorption in a refractive lens is usually taken into account using the magnitude of the linear absorption coefficient μ (see, e.g., Refs [19, 50, 51]), without the inclusion of phase-shifting properties of a material. A better-grounded criterion for the selection of refractive materials is the relation between their refractive properties and absorption [40, 47], represented by the characteristic number N_0:

$$N_0 = \frac{1}{\mu L_\pi} \, . \tag{6}$$

The number N_0 introduced here is rather simply expressed in terms of the refractive index decrements and atomic scattering factors. The quantity N_0 also defines the focal spot dimension [40] in the focusing of a plane wave (the diffraction limit of a lens):

$$\sigma_{\mathrm{F}} = \sqrt{\frac{F\lambda}{2\pi N_0}} \, . \tag{7}$$

We have compiled a database for the main parameters N_0 and L_π of the phase-shifting materials for X-ray refractive lenses, which were calculated from the atomic scattering factors in the photon energy range up to 100 keV for all chemical elements and more than 60 compounds [47]. The spectral dependences of material characteristics $\mu \propto \lambda^3$ and $L_\pi \propto \lambda^{-1}$, which enter into formula (6), are responsible for the corresponding behavior of the characteristic number $N_0 \propto \lambda^{-2}$. Our analysis suggests that the hard radiation range with photon energies above 10 keV, where the highest values of $N_0 > 50-100$ are reached for the materials with the effective atomic number $Z_{\mathrm{eff}} \leqslant 14$, is preferable for X-ray refractive lenses. In this case, a further growth of the values of L_π and N_0 occurs for photon energies above 30 keV. Therefore, the advantages of refractive lenses may be amply realized in the wavelength range where the capabilities of other types of X-ray focusing optics [12, 16] are limited.

One of the best materials from the viewpoint of the criterion introduced above is diamond which possesses the refractive index decrements $\delta = 5.07 \times 10^{-6}$ for a photon energy 12 keV, and $\delta = 2.92 \times 10^{-8}$ for 50 keV. Synthetic diamond single crystals hold considerable promise for the development of SR X-ray optics [55]. The perfection of synthetic diamond was studied [55] by the methods [56–58] of X-ray topography and optical fluorescence excited by an SR beam. It should be emphasized that the employment of diamond single crystals is preferred over the use of polycrystalline layers prepared by chemical vapor deposition [25, 59]. The diamond layers are sufficiently thick for the fabrication of refractive elements, but the parasitic scattering of the transmitted wave generated therein (see Ref. [49]) destroys the useful diffraction pattern.

To form single lenses with a radius of curvature $R \leqslant 1$ μm, use is presently made primarily of silicon and polymer materials, which is due to the possibility of resorting to a wide range of technologies exploited in microelectronics. Silicon refractive elements are practically void of intrinsic imperfections and, hence, do not give rise to their associated intensity losses.

2.3 Single parabolic short-focus lenses

We have made single parabolic lenses [48, 60, 61] from silicon by the technology of deep photoanodic etching. The parameters of the refractive profiles (paraboloids of rotation) of the lenses (Fig. 2) are as follows: radii of curvature $R = 0.35$ μm, aperture $A = 8$ μm, and the optical axis is perpendicular to the surface of the initial plate. The lenses were arranged in the form of a square matrix with the number of elements sufficient to intercept the cross section of the incident beam. The low absorption of the transmitted wave over the thickness of the lenses makes them closest analogs of visible-range lenses. Direct and statistical methods were developed for the quality assessment of the refractive profiles fabricated, and the focusing properties of the parabolic lenses were studied. The focal distances measured with a laboratory source range from 2×10^{-2} m for CuK_α radiation (8.05 keV) to $6.5-9.5 \times 10^{-2}$ m for MoK_α radiation (17.5 keV).

The properties of the single lenses fabricated were also studied with the ESRF synchrotron radiation source (Grenoble, France) in the 17–30 keV energy range (Fig. 2c) with recording on a high-resolution digital camera. The focal spot dimension did not exceed 0.7 μm. The measured focal distances corresponded to the calculated ones. The distinguishing features of these lenses were investigated in Refs [60, 61]. The focus dimension was evaluated with a submicrometer resolution and turned out to be close to the diffraction limit of resolution for these lenses; observations were made of the interference from two adjacent rows of the matrix, as well as of the self-reproduction effect (the Talbot effect) for the images of the focal-spot matrix. The lens matrix constitutes a high-quality two-dimensionally periodic optical element; its

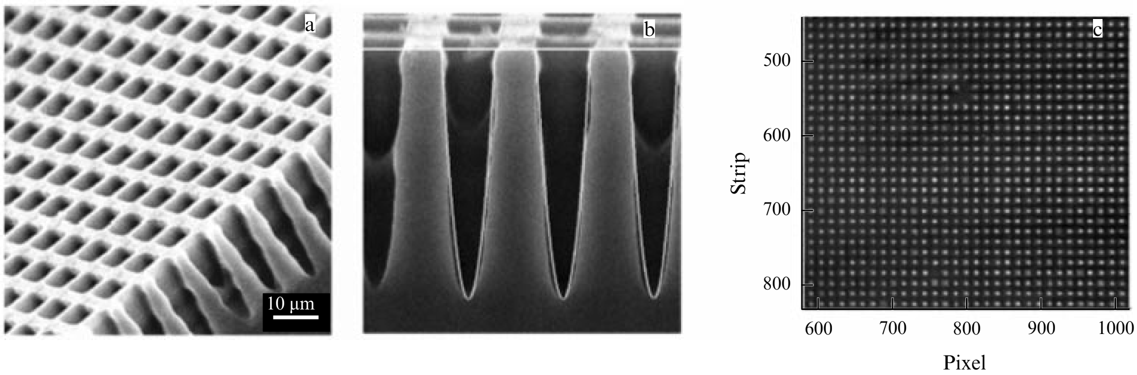

Figure 2. Short-focus parabolic lenses and radiation focusing by a lens matrix: (a) general view of the lens matrix; (b) refractive profile of a single lens with the optimal parabolic profile superimposed on it, and (c) photograph of the focal spots, obtained on the BM05 beamline at an energy of 30 keV.

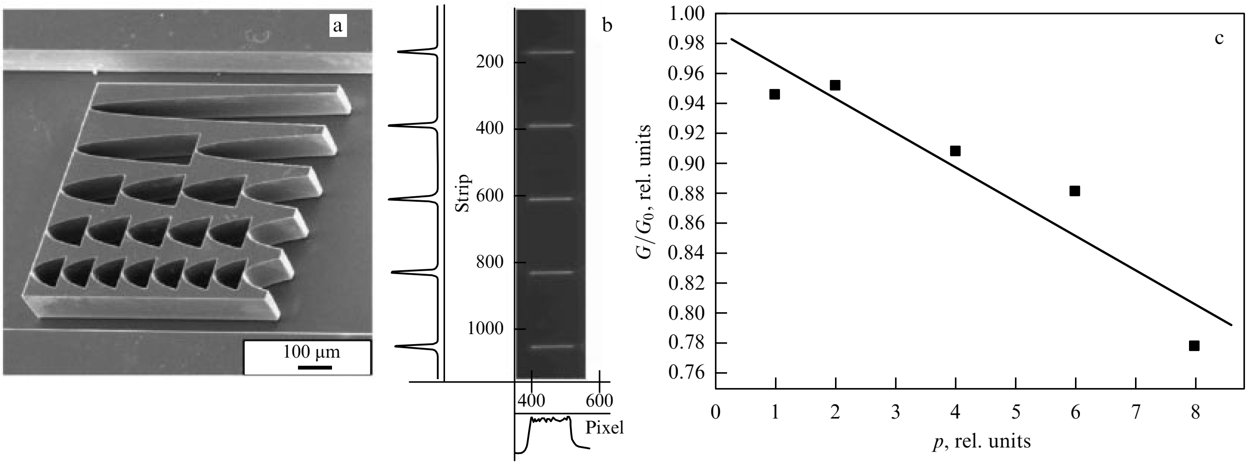

Figure 3. Planar parabolic lenses: (a) SEM image; (b) photograph of the focal spots, obtained on the BM05 beamline at an energy of 17 keV, and (c) planar lens gain versus set multiplicity according to measurements with SR .

capabilities in the analysis of perfection of photonic crystals were discussed in Refs [62, 63].

2.4 Planar lenses based on silicon and other materials

Let us consider the features and technology of fabricating planar lenses located on a plane substrate. Modern precision lithography technology permits forming the pattern of single lenses with sufficiently short radii of curvature also when the lens optical axis lies in the plane of the substrate. The refractive profile is made at the subsequent stages of lens fabrication, when the material may be removed from the inner part of the parabola or, alternatively, the requisite material is deposited onto its outer side. For the former variant we should first of all mention the deep etching of a silicon plate [64, 65]. The approach being described is the realization of the planar lens concept which has numerous aspects of development.

Silicon parabolic lenses (Fig. 3), which were first obtained in our work [64, 65], constituted a set of refractive profiles with equal focal distances of 1 m ($E = 17.4$ keV) and apertures $A = 100$ μm, and the multiplicity of the single lenses in a row increased from $p = 1$ to $p = 8$ with the corresponding growth in the radius of curvature R from 3.3 to 26.4 μm. The relief depth up to 100 μm was achieved by deep plasmochemical etching [64–66], and its increase is possible with the inclusion of the variation of the radius of curvature of the parabolas in depth [67]. The relief depth can also be doubled by way of the mechanical joining of planar lenses [25].

A property of the parabolic profiles shown in Fig. 3a is that the optical path of a ray and, accordingly, the total phase shift in traversing several lenses remain constant. The retention of the focal distance is ensured for all lens rows, which is confirmed by direct experimental measurements (Fig. 3b). The increase in the number of lenses in a row for a constant aperture is compensated for by a corresponding change in the radius of curvature. Accordingly, the lens power of a row is the superposition of the successive action of single lenses and is the same for all rows. Therefore, a sequential arrangement of single lenses with focal distances $F_0 \gg L$ — the overall longitudinal dimension of a set — clearly demonstrates the additivity of lens powers, similarly to the visible light optics [2]. The lens-power additivity of the refractive profiles follows directly from summation of the phase shifts produced by single lenses in the total phase shift acquired by the ray in transit through the set of profiles. The consequences of the property under discussion are discussed at length below.

The above lenses were investigated with laboratory [64] and synchrotron [65, 66] radiation sources. Measuring the intensities in their focal spots (Fig. 3c) [64, 65] allowed estimating by relation (2) the r.m.s. deviations of the profile from the ideal one. The resultant value of $\Delta Y = 0.45$ μm is indicative of a sufficiently high quality of the parabolic lenses fabricated, which underlies the diversity of their applications. In particular, they were employed [68] in the local diagnostics of heteroepitaxial films with recourse to the method of X-ray standing waves, which is outlined in greater detail below. The planar lenses were also utilized in the implementation of optical systems, including a beam condenser and a combined focusing system comprising a refractive lens and a planar X-ray waveguide [69], which are also described below.

Planar lenses were later fabricated in other laboratories as well. Mention should be made here of single parabolic lenses obtained by the X-ray lithography technique [70]. The planar silicon lenses described in Refs [71, 72] possess focal distances close to those of short-focus lenses.

Planar lenses made of polycrystalline diamond [59] were obtained by chemical vapor deposition of diamond layers onto silicon matrices under microwave discharge plasma excitation. The pattern of single parabolic lenses was preformed in the above matrices by precision lithography and plasmochemical etching techniques. The lenses possessed a focal distance of 50 cm for a photon energy of 9 keV. The experiments were carried out on the ID15 and ID22 beamlines at the ESRF using monochromatic radiation of the undulator third harmonic, as well as radiation with a continuous spectrum ranging from 6 to 40 keV. The lenses were able to withstand the thermal load under high-power irradiation with a power density up to 10 kW per square millimeter. Linear focal spots with a lateral dimension of 1 – 2 μm were obtained. The methods of phase contrast, small-angle scattering, and Debye spectra recording were applied when estimating the microstructure of the lenses. The lenses were shown to substantially broaden the energy range in which use can be made of refractive optics.

Planar lenses based on polycrystalline diamond layers were also reproduced in Ref. [26]. Mention should be made here of several works by Russian researchers dedicated to the fabrication of planar lenses on the basis of glassy carbon and the study of their properties [73 – 77].

3. Compound refractive lenses

3.1 Various realizations of compound refractive lenses

The additivity property of the lens power for single refractive lenses, which was demonstrated in experiments [19, 20, 64], is borne out by the theory of compound lenses [21, 22].

For a set of refractive lenses with a multiplicity p, located tightly to each other, the lens power is given by

$$D = \frac{1}{F_0} = \sum_{i=1}^{p} \frac{1}{F_i} \,. \tag{8}$$

In the special case when the focal distances of identical single lenses are equal ($F_i = F$), it follows from expression (8) that

$$F_0 = \frac{F}{p} \,. \tag{9}$$

For sufficiently large p there occurs a substantial shortening of the focal distance of the lens set and a corresponding increase in the radius of curvature of the single lenses (a calculation of focal distances F is given in Section 3.3). Therefore, the technological difficulties in the formation of single-lens profiles with radii of curvature ranging between several micrometers and tenths of a micrometer, which earlier (see Refs [12, 40]) were the main hindrance to their fabrication, can be removed by taking into account the additivity property (8) of the set. It is also valid to note that the difference between the exact parabolic profile and cylindrical or spherical profiles becomes insignificant.

The experimental realization of compound lenses was first reported in Ref. [19] (November 1996), in which lenses in the form of cylindrical hollows were made by drilling bores in an aluminium block. The precision of set formation, primarily the coaxial alignment of the bores and the degree of their internal surface finish, allowed producing the effect of radiation focusing into a linear spot. It is noteworthy that compound lenses in different combinations of refractive profiles of circular shape had earlier been described in a patent [78]. The patent was applied as a Japanese national patent in 1994, while its international publication came about later (February 1997) than Ref. [19]. One of the first works on compound refractive lenses is Ref. [79], whose authors came up with an unusual sequence of operations for the fabrication of the optical element and which had never been realized.

At the present time, different versions of fabrication of compound refractive lenses with a cylindrical refractive profile are known [19, 80 – 82], and different low-absorption materials have been tried, including beryllium [20, 89, 90] and polymers [83, 84, 91]. Also known are compound lenses with a spherical profile in the form of a set of hollow spheres, which comprise gas bubbles in a liquid [92, 93]. The most advanced are the technologies for the fabrication of refractive profiles in the form of a paraboloid of rotation (Fig. 4) [88 – 90] through mechanical treatment.

Focusing of hard X-ray radiation with a photon energy of 100 keV was first demonstrated with the compound sets of silicon planar lenses, which we described in Refs [94, 95]. Subsequent realizations of compound planar lens sets were described in several works by other researchers (see, for instance, Refs [25, 71, 72]). Here, mention should also be made of lenses formed by X-ray lithography techniques, which ensure focusing into a linear [96] and point [97] focus for focal spot dimensions close to the diffraction limit [98].

It is pertinent to note that the additivity (8) of the lens power of a set manifests itself only for refractive lenses and is not inherent in other types of X-ray focusers. In particular, a set of contiguously arranged Fresnel zone plates corresponds to one plate of summary thickness [99]. However, a shortening of the overall focal distance is observed for a set of two Fresnel zone plates spaced at some distance [100], but maxima emerge on their optical axis, which correspond to combinations of the diffraction orders of the plates [99], thus limiting the set multiplicity.

3.2 Beam focusing and collimation by refractive lenses

Obtaining a focal spot with minimal dimensions has traditionally been regarded as one of the main applications of X-ray focusing elements. Here, refractive lenses offer several major advantages over elements reliant on the principles of diffraction or mirror optics. Furthermore, the thin lens approximation is also applied to compound lenses with a high multiplicity of the set for $L \cong F_0$, as shown in Ref. [21].

The shortest known dimensions of a focal spot, which are defined — in the framework of ray optics — by the focusing geometry, are achieved in microprobe schemes where $a \gg b$ and $b \cong F_0$. In the realization of this scheme [16] with

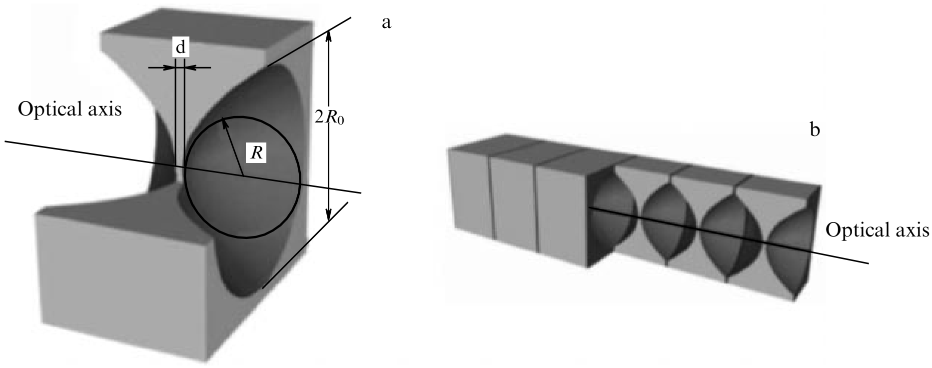

Figure 4. X-ray aluminium refractive lens with a double parabolic profile: (a) single lens (one quadrant of the lens is removed in the image); (b) single lenses arranged in a compound set. The geometrical lens aperture $2R_0 = 1$ mm, the radius of curvature at the tip of parabola is $r = 200$ μm. The r.m.s. roughness of the fabricated profile amounts to 0.1 μm [20].

synchrotron sources, where $a = 40-60$ m and $F_0 \approx 0.5-1$ m, the demagnification of a scheme may amount to 100–120 [16]. Therefore, for source dimensions of $s \leqslant 80-100$ μm, it becomes practicable to obtain a submicrometer focal spot with the sizes below 1 μm. Further lowering of focal spot dimensions is possible for lenses with short focal distances of 0.1–0.2 m, which guarantee the so-called nanofocusing of radiation [71, 72, 101, 102]. It should be remarked that it is only the FWHM of the linear focal spot of the planar lenses in the aforementioned papers that lies in the nanometer range. The length of the linear spot is defined by the profile depth (50–200 μm) of a planar lens, and the extent of a caustic region along the optical axis can be assessed at about 5–10 mm. In this case, the values measured in reality are substantially greater.

X-ray refractive lenses may be used to advantage as long-focus devices. In particular, a beam of parallel rays is assured when the focal distance of the lens is equal to the source distance. This scheme was first realized in Refs [84, 91]; compound lenses in the form of low-multiplicity sets were referred to as refractive collimators in order to emphasize their specific functions.

Silicon planar parabolic lenses [94, 95] were also employed as refractive collimators with a focal distance in the range of several dozen meters. In Ref. [103], the radiation beam collimation scheme based on these lenses was investigated with the ID15 beamline at ESRF. Figure 5 shows the arrangement of the elements of the setup, where the source–lens distance was equal to 61.7 m. To monochromatize the SR beam, use was made of a Si(111) monochromator in Laue geometry. In the experiment, the energy value E_0 was selected in such a way as to minimize the divergence of the output beam. For $E < E_0$, the lens forms a converging beam, and for $E > E_0$ a diverging beam from an imaginary source. A geometrical analysis for a point source showed that the calculated focal distance of the planar lens coincided with the source distance at $E_0 = 74.7$ keV.

To estimate the degree of beam collimation, Snigirev et al. [103] came up with an original technique for the direct measurement of output beam divergence, which does not call for resorting to complicated schemes comprising asymmetric crystal monochromators. According to this technique, a screen, which is a cloven Ge plate, is placed after the lens. The difference in position of the screen shadow in the direct beam and the beam transmitted through the lens (see Fig. 5) was measured from the image recorded by a FReLoN CCD camera (1.5 μm pixel size), when the screen was vertically scanned across the lens aperture within its effective aperture

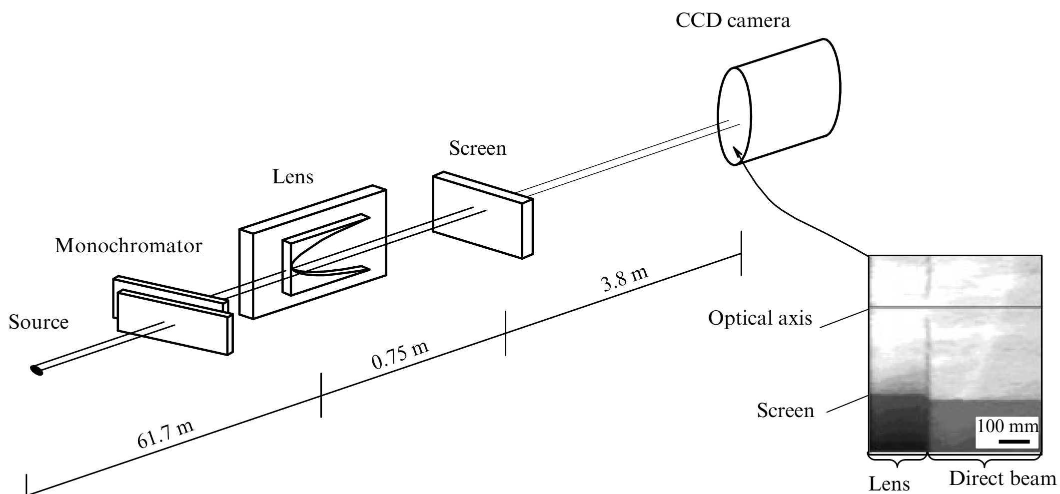

Figure 5. Schematic of the experiment on beam collimation by a planar lens. The inset shows the screen edge recorded by the CCD camera in the direct and lens-refracted beams.

(750 – 950 μm). According to the proposed method of calculation, the divergence angle of the output beam may be calculated from the screen image displacement for a given screen – image distance. A linear extrapolation of the experimental dependences obtained at $E_0 = 74.7$ keV yields a close-to-zero minimal slope coefficient. In this case, the residual angular beam divergence amounts to $\Delta\beta = 0.3$ μrad. The degree of SR beam collimation achieved in this case permits a substantial improvement in the angular resolution when studying the crystal-geometrical characteristics of multilayer epitaxial layers, in particular, latent heterojunctions in micro- and optoelectronic devices.

3.3 Properties of compound lenses as systems of single lenses

In the foregoing we directed attention to the fact that compound lenses may be regarded as 'thin' lenses only within certain limits. At the same time, they exhibit new properties as the systems of single lenses. The theory of compound lenses entering into high-multiplicity sets is outlined in Refs [21, 22, 104 – 111]. The main conclusions drawn from these investigations are given below.

Based on the statistical analysis of an ensemble of single lenses with random deformations and displacements from the common optical axis [21], it has been possible to determine their influence on the blurring of the focal spot and the output beam attenuation. The magnitude of their effect lowers as $\sqrt{p}$; in this case, the focal spot shape is hardly distorted by random displacements within the limits of the effective aperture of the compound lens for $p > 30$. A new property of the lens set is the displacement of the focal spot perpendicular to the optical axis on bending the compound lens through $L^2/3W$.

Introduced in Refs [22, 105 – 107] was a propagator function which defines the wave field distribution inside and behind the lens itself. With the inclusion of corrections expanded in powers of the small parameter L/F_0, it was shown that the focal distance of a compound lens measured from its center becomes equal to $F_0' = F_0 + L/6$. Compound lenses with an ultimately large-number set may be regarded as a continuous medium with a refractive index having a parabolic radial dependence [110, 111].

A compound refractive lens as a system of single lenses with a scale reduction of the radius of curvature constitutes a set in which the lens power of single lenses gradually increases from the input of the compound lens to its output. The requirement that the radius of curvature of single lenses be decreased stems from the narrowing of the wave front in the transmission of radiation through the compound lens [21, 22]. For these systems it is possible to attain a substantial shortening of the focal distance in comparison with compound lenses that comprise single lenses with a constant radius of curvature [66].

Relationship (6) in this case is written out as

$$\frac{1}{F_0} = 2\delta \sum_{n=0}^{N} \frac{1}{R_n} . \tag{10}$$

In the lens system under consideration we introduce a scale reduction of the radius of curvature R, which was earlier indicated in a patent [78]. For parabolic lenses, different versions may be selected to reach this goal, proceeding from the relation $Y = r^2/2R$ for geometrical parameters. For instance, for the corresponding variation of the lens radius, the scale reduction of the radius of curvature will be defined by the recurrent relationship

$$R_{n+1} = R_n q^2 . \tag{11}$$

Then, the focal distance of the lenses is defined by the sum of geometrical progression:

$$\frac{1}{F_0} = \frac{2Y\delta}{R_0^2} \sum_{n=0}^{N} \frac{1}{q^{2n}} . \tag{12}$$

As compared to compound lenses that have a constant value of the radius of curvature R, the lens systems under consideration ensure a significant shortening (up to 10-fold) of the focal distance at the same multiplicity of the set. According to relationship (10), for a set of 10 lenses this is achieved at $q = 0.83$, and for a set of 25 lenses already at $q = 0.93$. Decreasing the set multiplicity with retention of the focal distance of the systems being compared is another possibility. The aforementioned reduction effects are independent of specific values of the refractive index decrement for the materials of single lenses and are entirely defined by the parameters of the lens system and the scale factor. It is pertinent to note that the optimal values of the radius reduction factor are defined by the overall integral transmittance of the system. Lenses with a varied radius of curvature may ensure a gain in speed when the radius of curvature of the last lens in the set exceeds the effective one.

3.4 Technologies for the realization of compound refractive lenses with a downscaling of the radius of curvature

The realization of the above-considered lens systems with a scale reduction of the radius of curvature is a natural continuation of the conception of planar parabolic lenses outlined in the forgoing. We fabricated planar lenses [65] with two values of the scale factor: 0.93 and 0.97. For the same focal distance, this ensured the input lens radius increased in comparison with an ordinary planar parabolic lens. The refractive profile of the lenses fabricated (Fig. 6) had a relief depth of 200 μm. The data obtained in experiments with the laboratory source and the ESRF SR source confirm the advantages of planar lenses with radius-of-curvature reduction over conventional parabolic lenses.

It is worth noting that deep X-ray lithography, which is progressing at several scientific centers (see, for instance, Refs [96 – 98]), holds promise for the fabrication of the lenses under discussion.

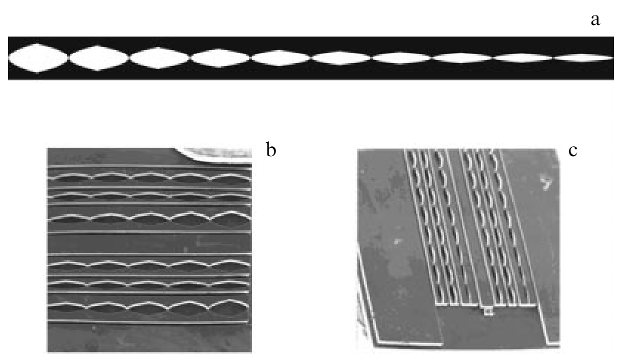

Figure 6. Set of silicon planar lenses with a scale reduction of the radius of curvature: (a) lens design; (b) SEM photograph of the input portion of the lens row, and (c) SEM photograph of the output portion of the lens row.

We came up with a new technology for fabricating a set of variable-radius-of-curvature lenses possessing axial symmetry. It relies on the principle of fixing the profile of a rotating liquid column [112], which is a parabola with a radius of curvature $R = 2g/\Omega^2$ [113]. For a conventional rotational speed (motor, 3000 r.p.m.), the radius of curvature turns out to be comparable to the figures afforded by relatively complicated techniques for mechanical formation [83 – 90]. Increasing the number of revolutions permits shortening the radius of curvature to the values obtainable by microelectronic technologies [64, 65]. Edge effects caused by the forces of surface tension distort the profile shape at the periphery, which is insignificant because of the strong absorption of the radiation passing through these segments. To obtain a set of lenses characterized by gradually decreasing radii of curvature, the rotation of a lens material holder is conducted at increasing rotational speeds

$$\Omega_n = \sqrt{\frac{2g}{R_0 q^n}}\,. \qquad (13)$$

The virtue of the technology under consideration consists in the simplicity of refractive lens formation and the absence of profile distortions and surface irregularities inherent in mechanical processing. Different ways [112] may be chosen to fix the profile in the solid phase. One of them represents photopolymerization of the materials possessing a perfect three-dimensional structure of a cross-linked polymer chain [114].

4. Refractive lenses with profiles derived from a parabola

4.1 Absorption-minimized parabolic lens

It should be borne in mind that in the X-ray band, unlike the visible region, absorption, which is exhibited even by light materials, should always be taken into account. Consequently, the peripheral regions of the above-discussed refractive lenses with a parabolic or circular profile, which lie outside of the effective aperture, make an insignificant contribution. To decrease absorption, it was suggested that the passive portions of the lens material in which the phase shift is equal to 2π should be removed so as to decrease, with retention of the phase variation law in the transmitted wave, its absorption, thus making it more uniform over the lens aperture [40]. In this case, the requirement that the function describing the refractive profile should be radially symmetric or even may be replaced with the same requirement imposed on the phase of the wave at the lens output: $\phi(x) = \phi(-x)$.

Absorption-minimized refractive lenses having a profile derived from a parabola were considered in Ref. [47] whose authors proposed technologies for their fabrication. Such lenses consist of a set of parabolic segments in which the phase variation in a transmitted wave is a multiple of 2π. In this case, the parabolic segments have a common generatrix (Fig. 7). This is a distinctive feature of the absorption-minimized silicon lens first created in our work [23].

The profile corresponding to a collecting lens with a real focal distance is described by the following expression

$$Y(x) = \left[\frac{L_\pi x^2}{F\lambda} - ML_\pi \operatorname{int}\left(\frac{x^2}{MF\lambda}\right)\right]. \qquad (14)$$

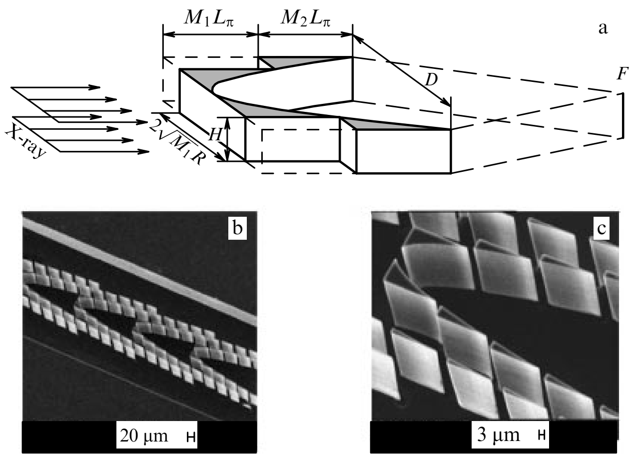

Figure 7. Absorption-minimized planar parabolic lenses: (a) focusing scheme; (b, c) SEM images of the resultant lens. *Notation*: D — lens aperture, H — profile depth, F — linear focus, M_1L_π and M_2L_π — segment dimensions along the beam direction.

Relationship (14) may be modified for a different instance when the segments have a convex parabolic profile, which corresponds to a divergent lens with an imaginary focal distance. It is pertinent to note that the formation of parabola-derived profiles implies the integration of individual profiles into a compound profile with the corresponding accumulation of lens power. From the above condition that the phase of the outgoing wave is even it follows that the tips of the individual profile segments may be inverted relative to the optical axis of the lens.

The realization of the kinoform profile with abrupt jumps between the boundaries of adjacent segments is fraught with serious technological problems when use is made of mechanical processing. Invoking modern microelectronic technologies and making planar refractive profiles [64] largely eliminate these difficulties [65 – 67].

In the absorption-minimized planar refractive lens [23] developed earlier on the basis of silicon (Fig. 7), the parabolic profiles with $M = 2$ are inserted one into another with a shift along the optical axis for a set multiplicity $p = 5$. In this case, the number of segment pairs equals 10, the base of the first segment measures 16.85 μm, and the lens aperture $A =$ 150 μm. The calculated focal distance is 0.8 m for a photon energy $E_0 = 17.5$ keV, which corresponds to the characteristic MoK_α line. The 90.5% transmittance of the lens at this energy far exceeds the transmittances of beryllium or aluminium compound lenses without absorption minimization [65].

The focusing properties of the lenses were studied experimentally with a laboratory source [64] and with the BM05 beamline of the ESRF SR source whose size was equal to 80 μm [115, 116]. In addition to a high-resolution digital camera, also mounted was a unit for precision slit scanning, which afforded a scanning pitch of 1 μm. The camera and the recording unit enabled measurements to be performed in the range of distances along the optical axis, which encompassed the entire interval of the depth of focus of the lens. The image of the focal spot produced by the lens does not contain subsidiary diffraction peaks. The data obtained in the experiment are in good agreement with calculated results. An analysis of the spectral properties of kinoform lenses is given below.

The type of lens [23] under consideration was subsequently reproduced in the works of several researchers [25–28]. To fabricate this type of lens with a profile of revolution, one may proceed along the avenues considered in our work [112].

4.2 Planar kinoform structures

A kinoform profile may be obtained by projecting the parabolic segments parallel to the optical axis of the lens, when their bases are located in a common line [47, 53, 65]. We emphasize that a virtue of the planar arrangement of the segments is the possibility of freely arranging them on a plane, without violating the phase relations. In Ref. [117] we considered the internal symmetry of kinoform refractive profiles; the corollaries of symmetry laws determine the possible types of parabolic segment arrangement on the plane in the design of planar profiles. The approach developed relies on the properties of point symmetry of X-ray stereoscopic imaging systems [118, 118]. The symmetry planes converting a unitary profile to itself serve as elements of the point symmetry subgroup for kinoform refractive profiles. Here, the symmetry plane perpendicular to the profile optical axis, whose introduction is necessitated by the principle of reversibility of the optical ray path, is black-and-white and turns over the segment apexes. It was determined that the minimal segment set invariant relative to the action of the symmetry planes corresponds to the profile with inverted apexes, and the rule of segments arrangement was derived. The simplest of these profiles are 'fern'-shaped profiles where the segment apexes alternately change their directions along the optical axis.

The kinoform lenses developed in our work are described in Refs [24, 53], which set out the experimental substantiations of their properties that are of significance to future developments. The conditions required for reproducing kinoform lenses by deep X-ray lithography techniques in the PMMA and SU-8 polymeric resists are defined in Ref. [120]. The specified lens formation procedures were carried out with the ANKA accelerator at the IMT synchrotron radiation center (Karlsruhe, Germany). Kinoform lenses with minimal segment sizes down to 1 μm for an aperture of 1.5 mm and a single-lens set multiplicity of 140 were produced (Fig. 8). The lenses formed in SU-8 resist layers were shown to possess a high radiation resistance and thermal stability. The focusing properties of these lenses were studied with the ESRF accelerator at a photon energy of 55.2 keV. Linear focal spots with a lateral size of 8.2 μm were obtained for a focal distance of 2 m. Subsequent work in this area allowed fabricating nickel kinoform lenses which were validly used to focus synchrotron radiation with an energy of 212 keV [121].

We emphasize that the above-outlined kinoform lenses exhibited the effects of wave field contraction immediately inside the lens, which were theoretically substantiated for smooth parabolic profiles in Refs [21, 22, 106]. In the case of kinoform lenses, these effects manifest themselves substantially more strongly, because the changes in the spatial characteristics of the wave fields in this instance are to be compared with the small dimensions of segment bases [122]. When the wave field contracts, the outermost segments of the profiles located near the lens output do not further participate in focal spot formation, which limits the ultimate multiplicity of compound kinoform lenses.

4.3 Analysis of the spectral properties of kinoform profiles

Let us analyze the spectral properties of kinoform lenses proceeding from the theory published in Ref. [117] and invoking the notions of X-ray crystallography. First of all, it should be mentioned that the compound-profile transformation group contains elements whose action (Fig. 9) reduces to the permutation of unitary profiles inside the common set. The function of subgroup generator is fulfilled by the operation of permutation of neighboring profiles, whose recurring actions multiplicate the unitary profile to the requisite set multiplicity. From the properties of the subgroup it follows that the action of the operators of its irreducible representation on the propagator retains its form, correct to the phase factor of the form $\Phi_m = \exp\,(2\pi \mathrm{i} m/L)$, and the propagator is the eigenfunction of the above operators.

The profiles under investigation are characterized by the existence of a set of intrinsic spatial frequencies with wave vectors which are multiples of the fundamental vector: $K_m = mK_0$. A coincidence of the optical length of any of the vectors of the set with the wave vector of a transmitted wave gives rise to peaks in the spectral dependences of the focal-spot intensity gain factor (Fig. 10). These lens properties were experimentally examined and were substantiated in the calculation of the amplitude transmission function by way of expansion in a Fourier series [23].

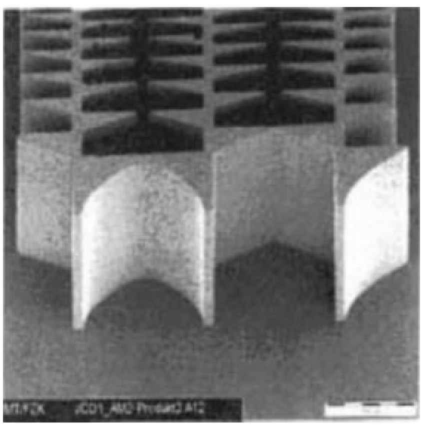

Figure 8. SEM images of a kinoform lens fabricated in PMMA [24].

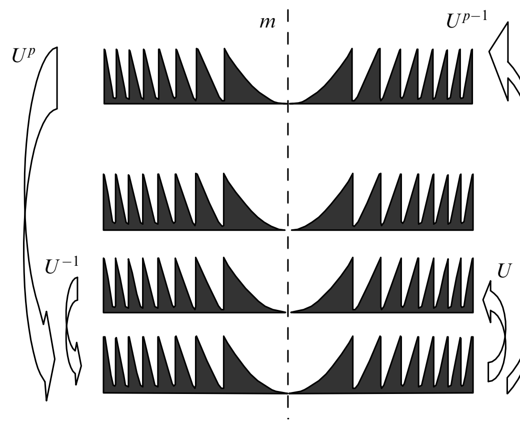

Figure 9. Arrangement of the elements of the permutation subgroup which enters into the kinoform profile symmetry group.

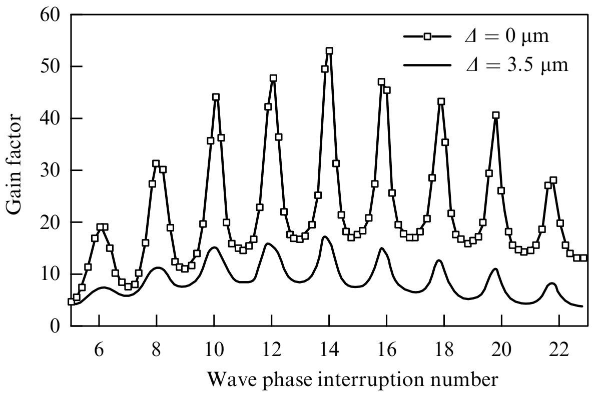

Figure 10. Gain factor as a function of diffraction order (the total number of wave phase interruptions over the total thickness of the lens material). Calculations were done for a silicon lens for radiation with an energy of $E_0 = 17.5$ keV. In the inset: technological resolution Δ. For an ideal lens, $\Delta = 0$ [23].

Therefore, kinoform lenses (as well as any of their versions, including lenses with minimized absorption) afford selective radiation focusing, which permits regarding them also as axial monochromators for the extraction of spectral radiation components along the optical axis [123]. The spectral resolution of an axial monochromator due to variation of the entrance slit width may amount to $\Delta E/E \cong 10^{-3} - 10^{-6}$, depending on the relation between geometrical parameters. The virtues of the axial monochromator are a high temperature stability and the absence of limitations at high energies, when the spectral resolution of the device under consideration does nothing but improve.

5. Refractive prisms and multiprism element sets

5.1 Spectral instruments based on refractive lenses

With the advent of compound refractive lenses, X-ray refractive optics became primarily a part of X-ray focusing optics. It is pertinent to note that lens optics by no means exhausts the variety of devices whose functioning relies on the refraction effect. First and foremost, mention should be made of devices based on prisms (Fig. 11) which ensure the rotation of beams or their resolution into spectral components. In this case, too, it is necessary to take into account the rather low value of the refractive index decrement for known materials and its strong dispersion (see Section 2.2) which is responsible for an appreciable lowering of the values of δ as radiation energy increases.

These physical limitations narrow the possibilities of employing refractive prisms in the X-ray band, where devices have already been developed for spectroscopic investigations involving single crystals with a spectral dispersion up to $\Delta E/E \cong 10^{-6}$ [12] and interference multilayer mirrors with $\Delta E/E \cong 10^{-4}$ [13, 16]. Nevertheless, the advent of new ultrahigh-power radiation sources [8, 9] and the shortening of pulse durations to femtoseconds [124] make the development of spectral devices employing refractive optical elements topical. The prism spectrometer of natural diamonds described in Ref. [125] ensures $\Delta E/E \cong 10^{-2}$, which exceeds the resolution of energy-dispersive detectors. Further improvement in spectral resolution is possible in more complex optical systems comprising other X-ray optical elements along with prisms.

Figure 11. Optical photograph of synthetic-diamond crystal prisms.

The angle of beam deflection upon traversing a refractive profile may be substantially increased due to the property of prism additivity, similarly to the power of single lenses in a compound lens. In this case, the total rotation angle

$$\varepsilon = \sum_{k=1}^{p} \varepsilon_k = \delta \sum_{k=1}^{p} \tan \frac{\alpha_k}{2} . \tag{15}$$

In particular, for similar rectangular blocks one has $\varepsilon = p\delta$.

5.2 Interference devices based on biprisms

The development of new devices for X-ray refractive optics enables broadening the range of its application and its capabilities by solving the problems specific to precisely the specified spectral range. Here, mention should be made of the problems of diagnostics of SR sources, which have become especially urgent in connection with the development of free-electron lasers. In particular, the diagnostics of an SR source [51], where images of the radiation-beam generation region were observed, became one of the first promising applications of X-ray refractive lenses. Direct information about the coherent properties of SR sources may be obtained in experiments that permit recording interference patterns (see, for instance, Ref. [126]).

X-ray biprisms made of crystalline silicon and synthetic diamond [58] were employed in experiments using the ESRF accelerator in studies of the coherent properties of the SR source at energies up to 30 keV (Fig. 12) [127–129]. Computer simulation techniques permit constructing an interference pattern in a biprism for different experimental geometries and a comprehensive evaluation of absorption in the biprism material and of the source dimensions. The calculated intensity profiles in interference fringes permit determining the dimension of the radiating region independently of the data obtained by direct observations of the source shape with the help of refractive lenses. The interference patterns for synthetic diamond biprisms were experimentally investigated with the ESRF BM05 beamline. The resultant images are in good agreement with calculations (Fig. 12).

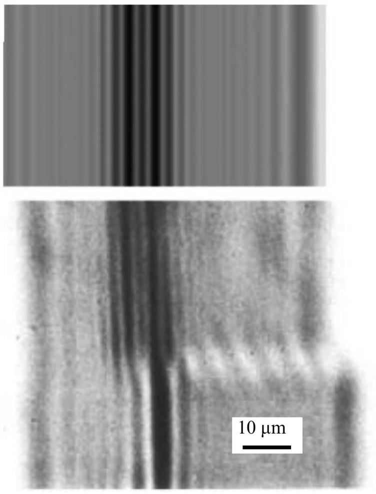

Figure 12. Interference fringes formed by a biprism in coherent radiation: (a) calculation; (b) observed fringes, and (c) fringes observed in interference with a single prism.

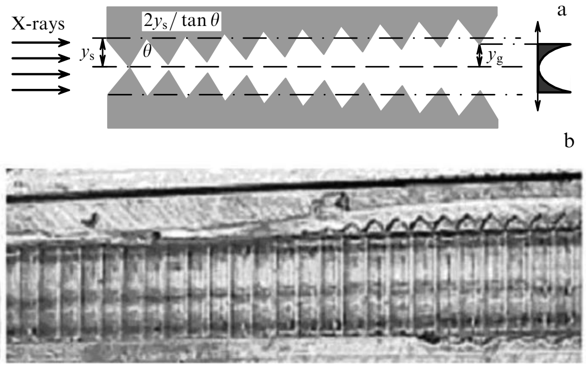

Figure 13. Multiprism element with a saw-tooth profile: (a) profile outline [46], and (b) photograph of two profiles with different pitches, made of lithium [130]. (Photograph courtesy of N R Pereira.)

Experimental techniques in combination with computer simulation techniques may be employed for the reconstruction of brightness distribution and mutual coherence functions in the radiating region, which is especially relevant to the latest generation of SR sources.

5.3 Multiprism focusing elements

The X-ray biprisms described above are a variety of refractive elements with a profile symmetric about the optical axis, where the profile continuity condition, as in the case of kinoform elements, is not fulfilled. It was shown that biprisms, in a number of cases, permit obtaining a rather intense central interference fringe with the depressed side fringes present. This capacity of biprisms is enhanced in multiprism refractive elements where symmetric sets are arranged on the basis of single prisms, the sets going into themselves under the action of the symmetry plane. It is pertinent to note that the multiprism elements under discussion possess a focal power corresponding to one parabolic lens.

The multiprism element described in Ref. [46] possesses a saw-tooth profile where prisms are symmetrically arranged, with their distance to the optical axis progressively increasing (Fig. 13). A light beam separated from the optical axis by a distance y traverses a path

$$Y(x) = \frac{x^2 N}{y_g \tan\theta} \qquad (16)$$

in the material of the element. Relationship (16) is the equation of a parabola with an effective radius of curvature

$$R_{\text{eff}} = \frac{y_g \tan\theta}{2N} \, . \qquad (17)$$

A saw-tooth profile enables obtaining a linear focus taking into account the focal distance defined by the radius of curvature R_{eff} and the refractive index decrement of the material [46]. The lateral dimension of the focal spot is defined by the demagnification factor of an optical scheme, while its limiting dimension in the focusing of a plane wave is defined by relationship (7), as in the case of parabolic lenses.

It is worth noting that multiprism elements afford moderate values of the focal-spot intensity gain factor, which are much lower than for parabolic lenses. Here, the main loss channels are the absorption in the optical ray path, the losses in multiple passes through individual prism surfaces, which possess random irregularities (roughness), and scattering in the material.

To realize this element, use was made of polymer materials [46] and lithium (Fig. 13b) [130, 131]. The main disadvantage of lithium is its high reactivity, with the consequence that the optical elements are enclosed in a shell filled with an inert gas [132].

Wedge-shaped passive material portions (Fig. 14) in multiprism elements may also be removed [30, 31], as was earlier demonstrated for parabolic lenses [23, 40]. Owing to this correction, the outer envelope of a multiprism element is, in the authors' opinion, sandwatch-shaped (clepsydra in ancient Greek).

The relations which describe the shape and arrangement of single prisms inside a clepsydra are largely similar to the relations derived earlier [23, 47] for the parabolic segments of kinoform lenses. First of all, it may be pointed out that the base length of single prisms along the optical axis $D_{\text{Cl}} = ML_\pi$ is a multiple of the phase shift length L_π. The height of the triangle in an individual prism is specified by the requisite focal distance and the design wavelength $\Delta Y_{\text{Cl}} = \sqrt{M\lambda F}$. The positions of individual prisms inside the clepsydra are defined

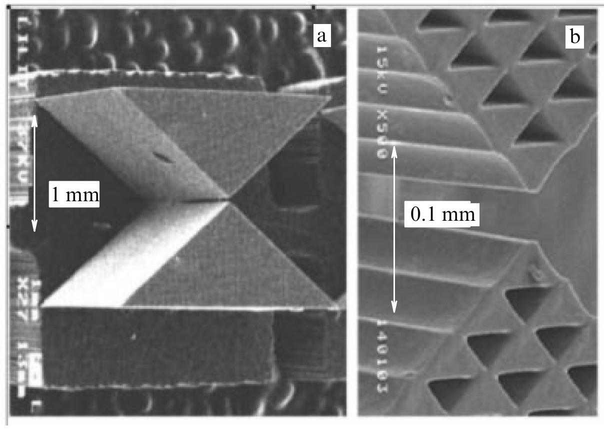

Figure 14. SEM images of a multiprism element with a clepsydra profile [30] fabricated by the X-ray lithography technique of PMMA: (a) overall view, and (b) central part. (Photograph courtesy of W Jark.)

by the coordinate reckoned from the optical axis: $Y_{\text{Cl}} = m_{\text{Cl}}\sqrt{M\lambda F}$.

The transmission of a series of prisms, unlike the case of parabolic segments (see, e.g., Refs [23, 24]), is described by a simpler expression

$$T(y) = \exp\left(-\frac{m_{\text{Cl}}M}{N_0}\right). \tag{18}$$

From relationship (18) it is possible to find the optimal row number and its corresponding value of the geometrical aperture of the multiprism element. The condition $T(y) = 0.75$ accepted by the authors of Refs [30, 31] leads to the expression

$$A_{\text{opt}} = 2.424\,N_0\sqrt{\frac{\lambda F}{M}}. \tag{19}$$

Therefore, an optimal aperture of the element is determined by material properties, the requisite focal distance, and the construction parameter of a clepsydra. It will be instructive to compare a clepsydra and a kinoform lens that have equal apertures and M numbers. First of all it may be pointed out, following the relations given in Refs [23, 24] and Refs [30, 31], that both the lens types have the same number of segments. In this case, the parabolic segments of the kinoform lens are equal to about half the height of clepsydra prisms.

The multiprism element design being described can function in the focusing geometry whereby the trajectories of incident and outgoing rays are approximately parallel to the element optical axis and the directions of the prism rows, which is valid in the 'thin-lens' approximation. At the same time, the sequential deflection of the transmitted ray by a series of prisms violates the applicability of this approximation. The effects of wave field contraction inside the lens itself were considered in Ref. [31]; similar effects had been known for long lenses with single parabolic profiles [20, 21, 106]. A geometrical analysis of ray deflection inside a clepsydra permits determining the admissible length of the prism row. The angle of ray deflection by the series of prisms is defined by relationship (13), while the linear ray displacement Δz may be found from expression (17) which defines the base dimension of the prisms. The ultimate row length in Ref. [31] is considered to be the number of prisms for which the above displacement becomes equal to the prism height defined by formula (18), and the refracted ray no longer participates in the formation of the focal spot. The maximum clepsydra aperture is limited in size to

$$A_{\max} = 2F\sqrt{2\delta}\,. \tag{20}$$

Therefore, the total aperture angle of a clepsydra is equal, in accordance with expectations, to the angle of total external reflection, like for Fresnel lenses based on elliptical segments [28].

It is noteworthy that the effects of wave field contraction inside a kinoform lens (see Section 4.2) manifest themselves to a substantially larger extent than for a multiprism element. However, the limitation on the set multiplicity for the kinoform lens is determined by the aperture angle and the refractive index decrement.

Multiprism elements (see Fig. 14) were fabricated in works [30, 31] by X-ray lithography techniques on the basis of PMMA and SU-8 polymeric resists. Taking into account the results of Refs [120, 121] on the fabrication of kinoform lenses from these materials, the minimal-height prism fabricated had a height of 12.83 μm, which specified the design-basis focal distance $F = 1.21$ m for a prism base length of 36.66 μm for the SU-8, and 40.66 μm for the PMMA. For a PMMA clepsydra with a doubled prism height and a doubled base length, the focal distance was twice as long: $F = 2.42$ m. The geometrical aperture of the fabricated elements was equal to 1.3 mm in all cases.

The fabricated elements were put to a test using the SYRMEP beamline of the ELETTRA accelerator (Trieste, Italy) [31] at an energy of 8.5 keV of monochromatic radiation for a lens – source distance of 22.6 m and a source dimension of 90 μm. The design-basis dimensions of the focal spot were equal to 11 μm for $F = 2.42$ m (5 μm for $F = 1.21$ m). The images obtained in the experiment possessed a substantial half-width of 40 – 60 μm for $F = 2.42$ m, and a somewhat smaller half-width of 35 – 50 μm for $F = 1.21$ m. The focal spots of the $F = 2.42$ m lenses were also recorded with the ID22 beamline of an ESRF synchrotron radiation source. The images obtained with improved resolution [30] disintegrate into several lines similar to the biprism interference pattern. Transmission measurements showed that the optimal aperture of the PMMA lenses coincided with the geometrical one, and it was equal to 0.93 mm for the SU-8 lenses. In summary, it is pertinent to note that the functioning of the elements produced depends on the contributions of technological imperfections in the course of their fabrication.

6. Two-lens systems

6.1 Beam condenser based on refractive lenses

A beam condenser ordinarily constitutes a two-lens scheme intended to change the beam geometrical dimensions. In the most common cases, use is made of two positive lenses. There are schemes where the first lens is positive, and the second one is negative. As follows from geometrical ray tracing (see Ref. [2]), in both cases the following relation applies:

$$\frac{A_1}{A_2} = \frac{F_1}{F_2}\,, \tag{21}$$

where A_1 and A_2 are the apertures, and F_1 and F_2 are the focal distances of the two lenses.

The outgoing beam compression may be achieved provided $A_1 < A_2$, so that the second lens should be short-focus. The distance between the lenses is equal to the sum of the focal distances for positive lenses, and to their difference for lenses of different types. In the latter case, it is possible to bring the lenses closer together and decrease the overall dimensions of the scheme.

The divergence of a beam emanating from a condenser is given by the angular source dimension, hence one has

$$\gamma = \frac{\Delta F_1}{F_2}\,, \tag{22}$$

where ΔF_1 is the linear dimension of the focal spot of the first lens. For a plane wave, γ is estimated as the angle for first-order diffraction by a lens aperture.

For a source of finite size, ΔF_1 will be its demagnified image, while for a microprobe scheme and $b \gg F$ one finds

$$\gamma = \frac{sF_1}{bF_2} = \frac{A_1}{A_2}\,\omega\,. \tag{23}$$

Relationship (23) is similar to the relation between the divergence and the geometrical beam dimensions, known for an asymmetric monochromator. It is noteworthy that the A_1/A_2 ratio in formula (23) may be replaced with the ratio R_1/R_2 between the lens radii of curvature in the important special case where both lenses consist of the same material.

Therefore, the resultant relation between the angles at the input and output of the condenser shows that the magnitude of γ is only specified by the condenser design parameters and is independent of the radiation energy. This property is a significant advantage of the condenser over a refractive collimator, where the collimation may actually be effected only for specific radiation energies.

The condenser throughput is determined by the integral transmission of both lenses, $T = T_1 T_2$. Hence, it follows that the second short-focus condenser lens should have a high transmission, and employing kinoform lenses may be among the optimal solutions to this problem.

In the experimental realization of beam condenser schemes, use was made of short-focus silicon refractive lenses with a transmittance of over 90%. In the setup involving a laboratory source, two lens matrices were arranged in series spaced at a distance $b = 2F = 14$ cm, the directions of their columns coinciding. The best resolution was observed at the output of the system ($B \approx 1$ cm) from the second lens. As the plane of recording was moved further away, the image produced by the matrices deteriorated and completely vanished at a distance $B = 20$ cm, which yields an estimate of $\gamma_{\rm expt} = \Delta F/B \cong 2\times10^{-5}$. In this case, it may be assumed that each lens in the matrix is irradiated by a beam with divergence equal to the angular source dimension $\omega = s/a = 1.9\times10^{-5}$. When this value is substituted into relationship (23), considering that the focal distances of the lenses are equal in the condenser model being described, we have $\omega = \gamma_{\rm expt}$. It is noteworthy that the resultant values of the outgoing-beam divergence angle at a level of $1-2\times10^{-5}$ rad are quite close to those which may be provided only by perfect-single-crystal collimators in their Bragg plane. In the condenser model being described, these values of divergence angles are retained in any plane passing through the beam, independently of its orientation. In this case, as in the case of beam collimation by one refractive lens, the direction of the primary beam is retained, which is highly significant in the practical employment of these schemes.

A two-lens condenser scheme, whose characteristics were measured with the BM05 beamline of the ESRF SR source, consisted of a planar lens and a matrix of short-focus lenses whose properties were discussed in the forgoing (see Fig. 2). In the photograph of the beam emanating from the condenser one can see that the focal spots of short-focus lenses are superimposed on the focal spots of the planar lens. We emphasize that the 100-μm aperture of this lens did not allow applying the above-outlined technique for the precision measurement of divergences by scanning an opaque screen across the lens aperture. Divergence measurements were performed by the method developed for a condenser prototype. According to the estimates of output beam divergence, obtained in the course of an experiment in the 8–25 keV energy range, the value of divergence angle $\gamma \cong 2\times10^{-5}$ remains invariable to within experimental error. In this case, this value is consistent with the value calculated by relationship (23) for the following ratio between the radii of curvature of both lenses: $R_1/R_2 \cong 10$. Therefore, an experimental verification of the characteristics of the two-lens condenser confirmed the relation derived.

6.2 System combining a planar lens and a waveguide

A combined system based on a refractive lens and a planar waveguide with an air gap [69] is of interest as a source of high-brightness submicrometer-sized beams. X-ray waveguides [32–36] belong, like refractive optics, to the rapidly developing area of high-resolution X-ray optics. Planar waveguides for X-ray radiation are a structure made up of thin films, where the transparent layer is confined between the reflective layers [32, 33]. An important waveguide application area is the formation of an outgoing beam with a submicrometer-sized cross section for conducting a local analysis of internal stress and elemental composition, with a lateral resolution in the 100-nm range, as well as for obtaining phase-contrast images. The tempting idea of achieving two-dimensional focusing in the nanometer range was realized with so-called two-dimensional waveguides [37], which suffer from extremely low throughput.

The absorption of radiation in the waveguide layer substantially restricts the possibilities of their application, decreases the output-beam compression coefficient relative to the primary beam, and impairs the conditions for single mode excitation [32, 33, 36]. The use of thin-film waveguides with a transparent beryllium layer was recently proposed [133] to lower the radiation absorption. In this respect, the arrangement of reflective blocks with a submicrometer-sized air gap in between seems more preferable. This version was realized in the form of separate blocks with a rather complicated mechanical alignment system for making an air gap of about 650 nm [36]. The construction of the waveguides of this type, described in Ref. [35], where the air gap between the reflective blocks is ensured by a thin-film separator, is much more simple, thus underlying its promise.

In the system realized in Ref. [69], the construction of a waveguide with an air gap involved the use of magnetic materials for the approach of reflective blocks (Fig. 15). A 10-mm-long waveguide channel of thickness 0.1 μm was

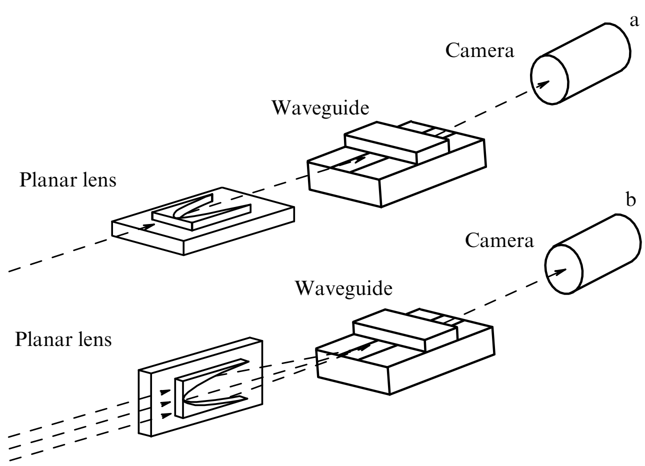

Figure 15. A schematic of the experimental arrangement for the combined focusing systems involving a planar lens and a waveguide with an air gap.

formed between upper and lower silicon plates separated by an Sm – Co alloy spacer with magnetization perpendicular to the substrate. These plates are pressed together by permanent magnets.

The experiment was carried out for two mutual arrangements of the refractive lens and the waveguide (see Fig. 15). The outgoing beam was recorded with a FReLoN CCD camera with an image element size of 0.8 μm. For a refractive lens, use was made of a planar silicon lens (see Fig. 3).

In the experimental arrangement of Fig. 15a, the focused beams passed through the waveguide channel and arrived at the input camera window. Therefore, this configuration is similar to the two-dimensional focusing scheme referred to as the Kirkpatrick – Baez system. We emphasize that for the second element, which effects the beam compression in the direction of the normal to the plane of the lens, use is made of a waveguide. The quantization of intensity in the form of peaks located along the linear focus is clearly seen in the resultant images of three parallel lens focal spots. These sets of intensity peaks correspond to the waveguide modes excited in this configuration. Since the peaks are equidistant, the spacing between any two of them may serve the purpose of estimating the angular interval $\Delta\Theta$ which separates the modes in the angular reflection spectrum of this waveguide. It is noteworthy that the thickness of the waveguide layer in thin-film waveguides unambiguously defines its angular reflection spectrum. However, a waveguide design using the pressing of two reflective blocks calls for an independent estimate of the interblock gap which represents the lateral dimension of the waveguide channel. The spacings between the neighboring peaks were next used to estimate the real gap size. The waveguide mode pattern is substantially simplified even for a rotation of the waveguide by the angle $\Delta\Theta$ specified above. The large number of excited modes recorded in the initial position reduces to two active modes which are substantially more intense than the rest of the modes.

In the arrangement of Fig. 15b, the planes of the lens and the waveguide were crossed, so that the lens focused the beam directly onto the input of the waveguide channel. In this case, the influence of the lens on the mode composition turned out to be even stronger. The factor of beam compression by the waveguide, calculated according to the accepted definition (see, for instance, Ref. [133]), was used to numerically estimate this influence. According to the measurements conducted, the strongest effect of lens focusing was observed for a waveguide with a length of the waveguiding channel of 6 mm. We emphasize that, according to the measurements, the fabricated waveguides possessed rather high values of the beam compression factor, which are appreciably higher than the values obtained for thin-film waveguides.

The aforementioned changes in conditions of waveguide illumination by a focused beam with an angular width governed by the aperture angle of the focusing element were studied in Ref. [134], where use was made of a linear Bragg – Fresnel zone plate. Increasing the zone-plate aperture led to a substantial growth in the beam compression factor, at the expense of losing coherent properties of a beam at the waveguide output. A transition from the single-mode regime to the multimode one was observed simultaneously. Our data on the realization of the single-mode regime under focused-beam illumination suggest that when use was made of a refractive lens, the coherence length of the initial SR beam persisted and, accordingly, so did the transverse coherence length for the outgoing beam.

Therefore, from the data outlined above it follows that it is possible to control the waveguide mode composition in the output beam with the minimal number of modes in the output beam being attainable. Refractive optical elements furnish the possibility of realizing combined focusing configurations that are simpler than the waveguide – zone plate combination [134].

7. Applications of refractive optics

7.1 Investigations with the beams formed by lenses

For laboratory sources, one usually has $a \leqslant 2-2.5$ m [60, 64], and the configuration demagnification coefficient ranges 8 – 10, which is an order of magnitude smaller than the above values for SR sources. Accordingly, the minimal obtainable size of the focal spot is equal to 5 – 10 μm. Notice that in this case a more compact solution to the focusing scheme problem for comparable focal spot dimensions may sometimes be furnished by other focusing elements which do not obey the lens law indicated above. In particular, reflective elements whose internal surface has the shape of a paraboloid of rotation enable collecting a polychromatic beam in a spot 10 μm in diameter in its geometrical focus, with the input end of the element arranged right up to the X-ray tube window [135]. The compactness of the focusing system and a sufficiently high radiation density ensure several successful applications for such elements, including those for local fluorescence [135, 136].

Fluorescence analysis comprising the excitation of secondary radiation by a focused X-ray beam was one of the first successful applications of Bragg – Fresnel zone plates [15, 16]. The employment for this purpose of compound refractive lenses [20] providing the focusing in the axial geometry permitted development of a new method for elemental analysis — microfluorescence tomography [137 – 140]. It was shown that the method being described enabled performing the three-dimensional reconstruction of the chemical element distributions in the sample under investigation. Several interesting results were obtained with its help. Mention should be made here of the analysis of particles ejected from the Chernobyl nuclear power plant, as well as of micrometeorites [139].

The focusing and collimation of radiation with the help of refractive optical devices may be regarded as two aspects of beam formation. While short-focus lenses are required to obtain a focal spot of minimal size, long-focus lenses are employed for collimation where the advantages of refractive devices are realized with relatively simpler requirements imposed. Such lenses may be treated as a reliable device which transforms the input beam with a divergence at a level of $10^{-3}-10^{-2}$ rad to the output beam, with maybe a divergence of less than 1 μrad. The additional advantage of refractive collimators over asymmetric crystal monochromators which guarantee comparable values of the angular divergence is that the incident and output collimator beams are coaxial.

Therefore, refractive optics may play the important part of matching crystal monochromators to an SR source, which was shown in several papers [84, 91, 141, 142].

The refractive collimator in Ref. [84] was made of PMMA and had a focal length of 45 m required for the BL47XU beamline of the SPring-8 accelerator (Japan). At the 18.5-keV radiation workstation, the design-basis transmittance of the fabricated collimator was equal to 75% owing to the large number of absorbing bridges between individual lenses. The efficiency of device operation was monitored by measuring the angular divergence of the output beam with the aid of a two-crystal system comprising silicon crystals mounted in the reflection position (+, +) for reflex (555). By measuring the half-width of the rocking curve under the rotation of the second silicon crystal it was determined that the angular divergence of the SR beam decreased from 11 to 3.5 μrad upon introducing the collimator. A drawback of the paper is the inexact determination of the operating focal distance of the collimator, which did not permit lowering the divergence to the rated value of 1 μrad.

Subsequently [91], refractive collimators were made of beryllium and aluminium, and an analysis was made of the factors that impeded the attainment of a better collimation. Notable among them were, apart from the aforementioned uncertainty in the determination of the source distance and the focal distance of the collimator, the finite angular source width, inaccuracies in centering the apertures in the compound lens, and the spherical aberrations of the fabricated cylindrical profiles.

The advantages of refractive collimators were more amply demonstrated in Refs [141, 142], where compound beryllium lenses (with a focal distance of 58.1 m at a photon energy of 14.41 keV) were employed in conjunction with a three-crystal scheme of asymmetric monochromators using the ID18 nuclear resonance scattering beamline at ESRF. The ultra-high energy resolution (better than 10^{-3} eV) requirement imposes strict limitations on the angular interval picked up by this focusing system from the incident synchrotron beam. Beam divergence at the input of the asymmetric monochromator block was lowered from 14 to 2.8 μrad upon introduction of the refractive collimator. A substantial (two-fold) gain in intensity was observed in this case.

7.2 Local structural and compositional diagnostics of crystalline materials

The local structural diagnostics of crystalline materials with the aid of beams focused by refractive lenses impose more stringent requirements than microfluorescence techniques. Here, the limiting factor is the focused beam divergence at a level of several milliradians, in accordance with the lens aperture angles. In this connection, the local structural diagnostics were performed primarily on polycrystalline materials where their application enabled obtaining new data at a microscopic level, which are important for materials science, solid-state physics, etc.

In Ref. [43], local structural diagnostics were employed to obtain more refined information about the mechanism of plastic deformation in zirconium. Zirconium constitutes one of the most important materials for nuclear reactors, and the work to study the relation between zirconium properties and its microstructure has been pursued since the 1970s. In Ref. [143], a study was made of plastic-deformed specimens of a zirconium-based alloy, which possess close-packed hexagonal structures. The experiment was staged with the ID22 beamline of the ESRF synchrotron radiation source, where the incident beam was focused by beryllium refractive lenses [90] on individual grains in a polycrystalline specimen. A map of grain orientations was preliminarily traced by means of electron backscattering technique, which allowed orienting individual grains to obtain the prescribed Bragg reflexes. Measurements were made of Debye line broadening for the purpose of estimating the dislocation density, the average subgrain size, and the activity of individual glide planes. It has been found that dislocations active in prismatic glide planes prevail in the plastic deformation process and their fraction in the total number of dislocations increases.

An investigation of critical fluctuations in microvolumes in the vicinity of the phase transition point, performed in Ref. [41], was made possible only owing to the use of focused X-ray beams. A theory is presently being elaborated that predicts the behavior of crystals near the phase transition point; however, experimental information on the transition mechanism at the microscopic level is extremely scarce. The available data on diffuse X-ray scattering in the neighborhood of the phase transition point, obtained with a macroscopic-sized incident beam, turn out to be insufficient for a detailed description of the transition at the microscopic level, making the local structural diagnostics a topical problem. In Ref. [41], theoretical predictions were made for the phase transition in an Fe_3Al alloy, whereby ordering of the positions of aluminium atoms at the center of a body-centered cell below $T_c = 700\,°C$ occurs. According to these predictions, studying the fluctuations that generate a new crystal phase requires, in view of their characteristic size and lifetime, concentrating the radiation in a volume with linear dimensions of 1 – 2 μm.

In the experiment staged with the ID22 beamline at ESRF, a study was made of Fe_3Al alloy specimens near the phase transition point [41]. Radiation with a photon energy of 16.5 keV was focused with a compound aluminium refractive lens to a spot 1.5 by 1.7 μm in size, which limited (in two dimensions) the size of the volume under investigation. The size in the third dimension, namely, along the lens optical axis, where there is a lengthy caustic region, was limited by the thickness of the specimen. For this purpose, advantage was taken of the technique of specimen preparation for transmission electron microscopy: a bore was etched in the sample under study. The beam was focused onto a thin portion of the wedge-shaped part of the specimen near this bore, where its thickness had the requisite value. Measurements were made of the (2, 2, 6) superstructural reflex of the ordered phase, where its intensity was equal to 10^3 pp s^{-1}. In the vicinity of T_c, intensity fluctuations exhibited the highest amplitude, which decreased upon receding from T_c within 0.05 °C. The manifestation of the λ singularity in the temperature dependence of the amplitude is an experimental confirmation of the universal laws of fluctuation dynamics in the critical region near the phase transition point for binary alloys.

We should also dwell on Ref. [42], which reported on the employment of a compound refractive lens for the structural analysis of hidden layers. The 70-keV radiation of the ID15A beamline at ESRF was focused onto a spot 5 by 15 μm in size on the plane interface between an ice layer and carbon dioxide. The specimen under study was placed in a low-temperature chamber with temperature stabilization. The experiment was performed using heating from −25 to 0 °C. The focused beam was incident on the side face of the specimen, traversing along the interface under investigation. Based on the analysis of scattering intensities, it was found that a quasiliquid spacer up to 5 nm in thickness forms at the ice – carbon dioxide interface, which is characteristic of ice premelting below the freezing point of water. The liquid density in the spacer was determined to exceed the density of ordinary water by 20% and be equal to 1.2 g cm^{-2}. The resultant data are an important step in the understanding of the behavior of ice at the boundary with rock consisting primarily of quartz, and permit explaining the high glacier flow speed in the framework of the proposed basal slip theory.

Another example of the possibilities of analyzing hidden layer structures with recourse to refractive optics is provided by the results of Refs [68, 144], which were concerned with the study of heteroepitaxial films and invoked the method of X-ray standing waves. It is pertinent to note that the planar parabolic lenses developed earlier [64] ensure the local analysis of single crystals despite the aforementioned divergence of the focused beam. In the selected geometry of the experiment, the planar lens focuses the beam in the anti-Bragg plane, while the depth of lens relief governs the slit dimension of 100 μm, which is sufficient for the operation at preferred points of the reflection diffraction curve under conditions established by a synchrotron source (Fig. 16).

The method of X-ray standing waves possesses an extremely high sensitivity to the atomic composition of the crystals under analysis, along with the capability of indicating the impurity location, but does not offer sufficient spatial resolution. Employing a focused beam enables retaining the aforementioned advantages of the method and furnishes spatial (lateral) resolution corresponding to the level of X-ray microscopy. The potentialities of this method were demonstrated by the example of the composition and perfection analyses of heteroepitaxial $Al_xGa_{1-x}As$ films grown on a GaAs (001) substrate. The method was elaborated using the experimental ID22 beamline at ESRF. The plane of incident beam diffraction by the crystal was taken to be horizontal, which permitted introducing a planar refractive silicon lens between the monochromator and the crystal. The beam was focused onto the end of a transverse cut of crystal, following which the beam was scanned within the thickness of the grown film. Topograms of the film and substrate segments were recorded simultaneously with the rocking curves and the intensities of fluorescence radiation of aluminium, gallium, and arsenic elements. The angular distributions of the outgoing fluorescence radiation correspond to the rocking curves recorded for a given segment. Therefore, the X-ray microscopy method with the excitation of standing X-ray waves may be employed for the elemental and structural layer-by-layer analysis of thin films and structures based on them.

7.3 Imaging in real and Fourier spaces. Photonic crystal research

X-ray image formation and transmission in real (direct) space without distorting the spatial frequency spectrum are important functions which may be fulfilled by focusing elements. In so doing, this first of all brings up the question of developing X-ray microscopy techniques for which the spatial resolution is determined by the ultimate resolution of the focusing element. During the last two decades, the above methods were implemented in the soft X-ray range using Fresnel zone plates (see Refs [12, 145]) and mirror optics [146]. It is noteworthy that two-dimensional images in X-ray microscopy are obtained with soft radiation (energies up to 1 – 1.5 keV), where the absorption depth (less than 1 μm) is only slightly greater than the resolution amounting to 20 – 100 nm.

In the hard X-ray range (from 6 – 10 to 100 keV), in which refractive lenses function, the absorption depth may far exceed the lens resolution. It should also be borne in mind that refractive lenses, which enable obtaining a submicrometer-sized focal spot, have a depth of field on the order of 0.1 – 1 cm. Any two-dimensional image recorded with their aid is projective with the imposition of details located lengthwise the beam path. Therefore, the correct interpretation of these distributions is only possible with the use of computer tomographic techniques (see, for instance, monographs [147, 148]).

To transfer X-ray images in real space, advantage is presently taken primarily of refractive lenses with an axially symmetric parabolic profile [20, 90]. There are pioneering reports about the employment of crossed planar lenses formed by X-ray lithographic techniques [96, 97] to transfer phase-contrast images [149]. We emphasize that capillary lenses with a spherical refractive profile [92, 93] exhibit significant aberrations which substantially distort the image. Preliminary focusing of the incident beam to decrease the lateral section of the projection in a tomographic scheme [150] may be the concrete area of applications for these lenses.

In recent years, rapid strides have been made by lens-free computer tomographic techniques for the three-dimensional image reconstruction of object structures. The development

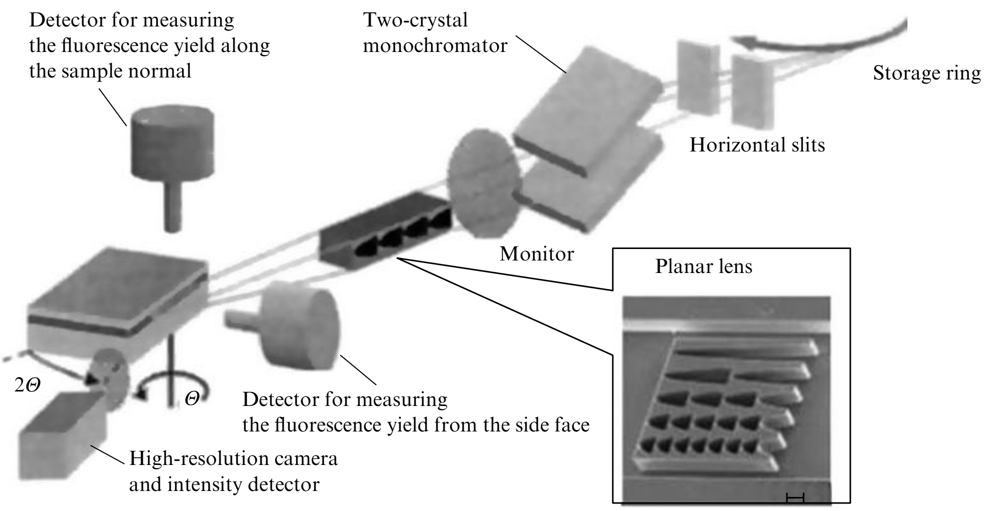

Figure 16. Local diagnostics using the X-ray standing wave technique with focusing effected by a planar lens. Inset: SEM image of the lens [68].

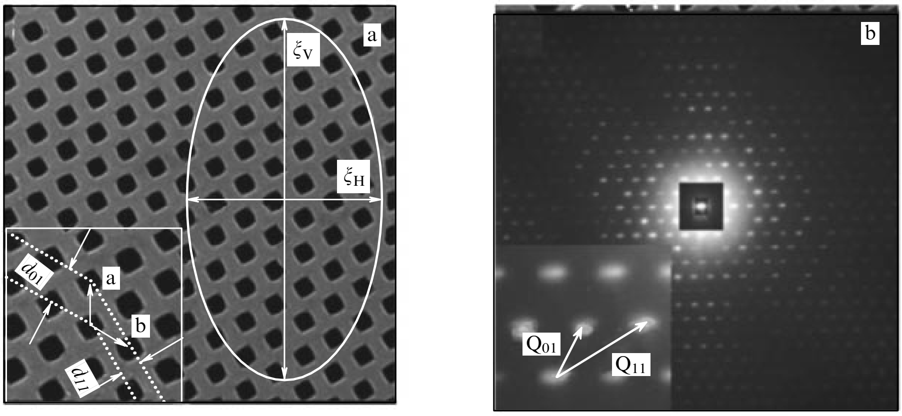

Figure 17. X-ray diffraction by a photonic crystal, recorded with the help of a refractive lens [157]: (a) SEM image of a segment of the photonic crystal (inset: translation vectors of an elementary cell of the photonic crystal are $a = b = 4.2$ μm; the dashed lines indicate the d_{01} and d_{11} interrow spacings). The enclosed zone corresponds to the domain of coherent illumination of the given segment, which is specified by the spatial coherence lengths in the horizontal (ξ_H) and vertical (ζ_V) directions; (b) diffraction pattern recorded in the rear focal plane of the lens at a photon energy of 28 keV. Inset: vectors of the reciprocal lattice for two main reflexes. (Photographs courtesy of M Drakopoulos.)

of X-ray tomography for microobjects commenced in Russia in the mid-1980s have now led to the advent of nanotomographs with a resolution as high as 200 nm [151]. Further improvements in the resolution of these instruments for the analysis of nanoobjects is foreseen. The techniques of nanoobject image reconstruction from diffraction spectra in the Fourier space [45] possess certain potentialities for the derivation of three-dimensional pictures with a resolution at a level of 25 – 50 nm.

Compound refractive lenses with an axially symmetric parabolic profile [20] enabled transmitting the undistorted shadow images of the simplest test objects. Subsequently, the high quality of these lenses turned out to be the decisive factor in the development of methods for producing the Fourier images of artificial periodic structures like photonic crystals. The photonic crystals are two- or three-dimensional periodic structures which acquire extraordinary optical properties in the wavelength range close to the period of a given structure [152, 153], where an energy gap is observed in their optical spectra. Particularly interesting and promising from the standpoint of optoelectronic applications are the photonic crystals fabricated from silicon on the basis of modern technologies [154 – 156]. The necessity of monitoring the quality of photonic crystals, which is reflected in their main properties [63], underlies the significance of the X-ray techniques intended for investigating their perfection.

Refractive X-ray lenses may be employed, as shown by the theoretical analysis of Refs [105 – 109], as a tool for producing a diffraction pattern with a high angular resolution, which permits investigating the long-range order in periodic structures. These properties correspond to the employment of lenses in optics, where the Fourier image of an object is also obtained at the rear focal plane. Notice that in this case the lenses of both types produce a pattern integral (averaged) over the object area, unlike the local investigations with focused beams, where the domain under investigation is limited.

The periodic structures of photonic crystals were analyzed [157] with the ID18 beamline of the ESRF synchrotron source. The object in Ref. [157] was a photonic crystal (Fig. 17), which comprised a hexagonal mesh of pores etched in a 150-μm-thick silicon crystal. The pores had the shape of a square with a 2-μm-long side, with the length of translation vectors of the hexagonal mesh being equal to 4.2 μm. This object was arranged immediately at the output of a compound aluminium parabolic lens, and the diffraction pattern was recorded with the help of a high-resolution CCD camera, with the two-dimensional detector located at the rear plane of the lens at a distance of 1314 mm from it.

The observed diffraction pattern (Fig. 17b) represented a set of spots located at the sites of a reciprocal lattice with a hexagonal symmetry. In this experiment, 12 diffraction orders with the coherence area shown in Fig. 17a were recorded. The distances between the closest reflexes are proportional to the length of the minimal vector of the reciprocal lattice (inversely proportional to the lattice spacing). The dimensions of individual spots and their structure — the structure of a reciprocal lattice site — carry information about the photonic crystal perfection. The instrumental error as the contribution of the measuring scheme, obtained from the diffraction pattern, is determined by the angular source size and the wave vector of the incident wave, which is estimated by the magnitude of $\Delta k = 1.42 \times 10^{-4}$ nm^{-1}. The aforementioned characteristics of the diffraction pattern, which is obtained with the help of an X-ray refractive lens, testify to the high accuracy in determining the photon-crystal lattice spacing $\Delta d/d \approx 4 \times 10^{-3}$, which is close to the values furnished by X-ray structure analysis techniques in the measurement of real crystals.

It is pertinent to note that the method described in Ref. [157] permits determining the integral characteristics of an object under investigation and applies to a sufficiently perfect photonic crystal. Variations in the pore mesh period result in a blurring of the diffraction pattern and the corresponding lowering of the accuracy in lattice spacing determination.

We also point out that the use of self-reproduction of periodic structures (the Talbot effect), which was observed with a two-dimensional array of short-focus lenses in our earlier work [61, 62], is of certain interest in the study of the two-dimensionally periodic structure of photonic crystals.

8. Conclusions

X-ray refractive optics, which came into being about 10 years ago, has turned into a branch of modern optics in its own right, and relies on the firm basis of theoretical investigations and experimental evidences. It is noteworthy that its advancement has taken place in intense competition with other types of focusing optics. Refractive optical elements and devices possess a new combination of properties and characteristics, which enables them to fulfill a broader set of functions in comparison with other X-ray optical elements. In particular, it is likely that X-ray compound lenses are the tool of choice for the elemental and structural analysis of thin films and composites based on them, analysis of hidden layers, the investigation of synthesized periodic structures like photonic crystals, etc. The applications of refractive lenses (as with other X-ray optical elements) to the transmission and transformation of X-ray images rely on X-ray tomographic techniques.

X-ray astronomy may become a new application area for refractive optical elements. The range of hard X-ray radiation is thought of as being potentially promising for progress in understanding a number of astrophysical problems. As of now, the data on deep probing of the Universe in this spectral range are practically nonexistent due to the stringent requirements imposed on the sensitivity of the telescope and its angular resolution. Other requirements connected with the telescope are a very broad radiation energy interval recorded (up to 600 keV and higher) and a large field of view of dozens of angular degrees. An analysis of publications [158–169] suggests that refractive elements offer several advantages over the elements of reflective and zone optics in the design of a powerful X-ray telescope. Mention should be made here of the feasibility of making focusing instruments with long focal distances. At the same time, refractive elements allow their fabrication requirements to be greatly eased in comparison with the elements of reflective and zone optics and ensure their serviceability under extreme conditions aboard a spacecraft.

The findings of research into the physical foundations and design principles of refractive lenses have already found rather wide application. Further progress in this field involves the search for new designs of the elements and their fabrication technologies, as well as the development of combined and multicomponent systems.

Acknowledgments. The authors express their appreciation to Prof. V G Kohn for the helpful remarks. This work was supported by the Russian Foundation for Basic Research under grant No. 07-02-12064.

9. List of symbols

A — aperture of a focusing element (a lens)
A_{eff} — effective aperture of a focusing element (a lens) with the inclusion of absorption
$A_{\max}$ — maximum aperture of a focusing element (a lens)
A_{opt} — optimal aperture of a focusing element (a lens)
a — source–lens distance
B — distance to the recording plane measured along the optical axis
b — lens–image distance
D — lens power of a set of lenses
D_{Cl} — base length of single prisms along the optical axis
d — interplane distance
Δd — interplane distance variation
E — radiation energy
F — focal distance of a single lens
F_0 — focal distance of a set of single lenses
G — focal-spot intensity gain factor
g — acceleration of gravity (9.81 m s^{-1})
H — profile depth of a planar focusing element (a lens)
I — radiation intensity
I_0 — incident beam radiation intensity
ΔI — change in radiation intensity
K — spatial frequency wave vector
K_0— fundamental wave vector of a spatial frequency set
K_m — wave vector of a spatial frequency set
k — radiation wave vector
L — length of a set of single lenses measured along the optical axis
L_π — path length for a wave phase shifted by π
l — optical path difference between a parabola and the approximating segment
M — even number of phase variations in the segment of a parabolic lens
m_{Cl} — single-prism row number
N — number of prisms
N_0 — characteristic number
n — refractive index
p — multiplicity of a set of single lenses
q — scale reduction factor in a set of single lenses
q_0 — optimal value of the scale reduction factor
R — radius of curvature at the vertex of a parabola
R_0 — initial radius of curvature in a set of single lenses
R_{e} — equivalent radius of curvature in a multiprism element
r — radial coordinate
s — source size
T — integral transmittance of a focusing element (a lens)
T_{c} — phase transition temperature
U — operation of element permutation in a compound lens
W — radius of bending of a lens set
x, y — Cartesian coordinates
$Y(x)$ — refractive profile shape
ΔY — root-mean-square deviation of a profile from the ideal one
ΔY_{Cl} — height of triangle in a single prism
Y_{Cl} — position of the vertices of single prisms in a 'clepsydra' profile
y_g — position of the vertices of prisms in a saw-tooth profile
Δy — random refractive-profile deviations
Z — atomic number of a chemical element
Z_{eff} — effective atomic number of a chemical compound
α — prism vertex angle
β — imaginary part of the refractive index
γ — beam divergence angle at the output of a focusing element (a lens)
$\varDelta$ — parabola approximation step
δ — decrement (real part) of the refractive index
ε — beam rotation angle upon traversing a refractive profile (a prism)
λ — radiation wavelength
μ — linear absorption coefficient
σ_F — diffraction limit of a lens
$\varTheta$ — angle in the reflection (diffraction) spectrum
θ — angle of prism base inclination relative to the optical axis
$\Delta\varPhi$ — maximum wave phase difference
$\varPhi_m$ — phase multiplier
ϕ — wave phase at the lens output
$\varOmega$ — angular rotational speed
ω — angular dimension of a radiation source

References

1. Roentgen W K *Nature* **53** 274 (1896)
2. Born M, Wolf E W *Principles of Optics* 7th ed. (Cambridge: Cambridge Univ. Press, 1999)
3. Blokhin M A *Fizika Rentgenovskikh Luchei* (The X-ray Physics) (Moscow: GITTL, 1953)
4. Aristov V V *Vestn. Ross. Akad. Nauk* **72** 963 (2002)
5. von Laue M *Ann. Phys.* (Leipzig) **41** 248 (1913)
6. Compton A H *Philos. Mag.* **45** 1121 (1923)
7. Tolfree D W L *Rep. Prog. Phys.* **61** 313 (1998)
8. What is a Synchrotron? http://www.esrf.eu/AboutUs/AboutSynchrotron
9. The European X-Ray Laser Project XFEL, http://xfel.desy.de
10. Vinogradov A V et al. *Zerkal'naya Rentgenovskaya Optika* (X-Ray Mirror Optics) (Executive Ed. A V Vinogradov) (Leningrad: Mashinostroenie, 1989)
11. Dabagov S V *Usp. Fiz. Nauk* **173** 1083 (2003) [*Phys. Usp.* **46** 1053 (2003)]
12. Michette A G *Optical Systems for Soft X-Rays* (New York: Plenum Press, 1986) [Translated into Russian: (Moscow: Mir, 1989)]
13. Bibishkin M S et al., in *Rentgenovskaya Optika-2004: Materialy Soveshchaniya, Nizhnii Novgorod, 2–6 Maya 2004 g.* (X-Ray Optics-2004: Conf. Proc., Nizhnii Novgorod, 2–6 May 2004) (N. Novgorod: Institute for the Physics of Microstructures, Russian Academy of Sciences, 2004) p. 198
14. Gaponov S V et al., in *Nanofizika i Nanoelektronika: Mezhdunar. Simpozium, 25–29 Marta 2005 g., Nizhnii Novgorod* (Nanophysics and Nanoelectronics: IX Intern. Symp., 25–29 March 2005, Nizhnii Novgorod) Vol. 2 (N. Novgorod: Institute for the Physics of Microstructures, Russian Academy of Sciences, 2005) p. 44
15. Erko A I, Aristov V V, Vidal B *Diffraction X-ray Optics* (Bristol: IOP Publ., 1996)
16. Dhez P et al. *Rev. Sci. Instrum.* **70** 1907 (1999)
17. Shchelokov I A et al. *Izv. Ross. Akad. Nauk, Ser. Fiz.* **68** 514 (2004) [*Bull. Russ. Acad. Sci., Phys.* **68** 582 (2004)]
18. Firsov A A et al. *Opt. Commun.* **202** 55 (2002)
19. Snigirev A et al. *Nature* **384** 49 (1996)
20. Lengeler B et al. *J. Synchrotron Rad.* **9** 119 (2002)
21. Kohn V G *Pis'ma Zh. Eksp. Teor. Fiz.* **76** 701 (2002) [*JETP Lett.* **76** 600 (2002)]
22. Protopopov V V *Opt. Commun.* **172** 113 (1999)
23. Aristov V et al. *Appl. Phys. Lett.* **77** 4058 (2000)
24. Shabel'nikov L et al. *Proc. SPIE* **4783** 176 (2002)
25. Nöhammer B et al. *Microelectronic Eng.* **67–68** 453 (2003)
26. Nöhammer B et al. *J. Synchrotron Rad.* **10** 168 (2003)
27. Evans-Lutterodt K et al. *Opt. Express* **11** 919 (2003)
28. Stein A, Evans-Lutterodt K, Taylor A *Proc. SPIE* **6002** 202 (2005)
29. Lang A R, Makepeace A P W *J. Synchrotron Rad.* **6** 59 (1999)
30. Jark W et al. *J. Synchrotron Rad.* **11** 248 (2004)
31. Jark W, Pérennès F, Matteucci M *J. Synchrotron Rad.* **13** 239 (2006)
32. Di Fonzo S et al. *Nature* **403** 638 (2000)
33. Pelliccia D et al. *J. Phys. D: Appl. Phys.* **38** A213 (2005)
34. Bushuev V A, Roshchupkina O D, in *Nanofizika i Nanoelektronika: Mezhdunar. Simpozium, 10–14 Marta 2007 g., Nizhnii Novgorod* (Nanophysics and Nanoelectronics: XI Intern. Symp., 10–14 March 2007, Nizhnii Novgorod) Vol. 1 (N. Novgorod: Institute for the Physics of Microstructures, Russian Academy of Sciences, 2007) p. 111
35. Egorov V K, Egorov E V *Appl. Surf. Sci.* **253** 138 (2006)
36. Zwannenburg M J et al. *Rev. Sci. Instrum.* **71** 1723 (2000)
37. Pfeiffer F et al. *Science* **297** 230 (2002)
38. Aristov V V et al. *Pis'ma Zh. Eksp. Teor. Fiz.* **28** 6 (1978) [*JETP Lett.* **28** 4 (1978)]
39. Indenbom V L, Slobodetskii I Sh, Truni K G *Zh. Eksp. Teor. Fiz.* **66** 1110 (1974) [*Sov. Phys. JETP* **39** 542 (1974)]
40. Yang B X *Nucl. Instrum. Meth. Phys. Res. A* **328** 578 (1993)
41. Mocuta C et al. *Science* **308** 1287 (2005)
42. Engemann S et al. *Phys. Rev. Lett.* **92** 25701 (2004)
43. Kuyumchyan A et al. *Proc. SPIE* **4783** 92 (2002)
44. Michette A G et al. *Opt. Commun.* **245** 249 (2005)
45. Darahanau A V et al. *Phys. Lett. A* **335** 494 (2005)
46. Cederström B et al. *Nature* **404** 951 (2000)
47. Aristov V V et al. *Poverkhnost': Rentgen., Sinkhrotron., Neitron. Issled.* (1) 7 (1999)
48. Starkov V V et al. *Poverkhnost': Rentgen., Sinkhrotron., Neitron. Issled.* (1) 146 (1999)
49. Shabel'nikov L G, in *Nanofizika i Nanoelektronika: X Mezhdunar. Simpozium, 13–17 Marta 2006 g., Nizhnii Novgorod* (Nanophysics and Nanoelectronics: X Intern. Symp., 13–17 March 2006, Nizhnii Novgorod) (N. Novgorod: Institute for the Physics of Microstructures, Russian Academy of Sciences, 2006) p. 404
50. Snigirev A A et al. *Proc. SPIE* **3151** 164 (1997)
51. Elleaume P *Nucl. Instrum. Meth. Phys. Res. A* **412** 483 (1998)
52. Snigirev A et al., in *Rentgenovskaya Optika-2004: Materialy Soveshchaniya, Nizhnii Novgorod, 2–6 Maya 2004 g.* (X-Ray Optics-2004: Conf. Proc., Nizhnii Novgorod, 2–6 May 2004) (N. Novgorod: Institute for the Physics of Microstructures, Russian Academy of Sciences, 2004) p. 62
53. Aristov V V et al. *Poverkhnost': Rentgen., Sinkhrotron., Neitron. Issled.* (1) 77 (2000)
54. Akhsakhalyan A A et al., in *Nanofizika i Nanoelektronika: Mezhdunar. Simpozium, 25–29 Marta 2005 g., Nizhnii Novgorod* (Nanophysics and Nanoelectronics: IX Intern. Symp., 25–29 March 2005, Nizhnii Novgorod) (N. Novgorod: Institute for the Physics of Microstructures, Russian Academy of Sciences, 2005) p. 518
55. Härtwig J et al., in *Coll. Abstracts of 8th Biennial Conf. on High Resolution X-Ray Diffraction and Imaging (XTOP-2006), Germany, 19–22 September 2006,* TO4-2
56. Hosowska J et al. *J. Phys. D: Appl. Phys.* **34** A47 (2001)
57. Tamasaku K et al. *J. Phys. D: Appl. Phys.* **38** A61 (2005)
58. Borzdov Yu M et al. *Dokl. Ross. Akad. Nauk* **374** 91 (2000) [*Dokl. Earth Sci.* **374** 1113 (2000)]
59. Snigirev A A et al. *Proc. SPIE* **4783** 1 (2002)
60. Aristov V V et al. *Opt. Commun.* **161** 203 (1999)
61. Aristov V V et al. *Poverkhnost': Rentgen., Sinkhrotron., Neitron. Issled.* (1) 71 (2000)
62. Aristov V V et al. *Mikrosistemnaya Tekhnika* (8) 39 (2001)
63. Barabanenkov M Yu, Starkov V V, Shabel'nikov L G *Poverkhnost': Rentgen., Sinkhrotron., Neitron. Issled.* (2) 64 (2006)
64. Aristov V V et al. *Opt. Commun.* **177** 33 (2000)
65. Aristov V V et al. *Poverkhnost': Rentgen., Sinkhrotron., Neitron. Issled.* (1) 13 (2001)
66. Aristov V V et al. *Proc. SPIE* **4145** 285 (2001)
67. Snigireva I et al. *Proc. SPIE* **5195** 32 (2003)
68. Drakopoulos M et al. *Appl. Phys. Lett.* **81** 2279 (2002)
69. Shabel'nikov L G et al. *J. Phys. IV* (France) **104** 227 (2003)
70. Zhang Y et al. *Jpn. J. Appl. Phys.* **40** L75 (2001)
71. Schroer C G et al. *Proc. SPIE* **5539** 10 (2004)
72. Schroer C G et al. *Appl. Phys. Lett.* **87** 124103 (2005)
73. Artemiev A N et al. *Nucl. Instrum. Meth. Phys. Res. A* **543** 322 (2005)
74. Artem'ev A N et al. *Poverkhnost': Rentgen., Sinkhrotron., Neitron. Issled.* (2) 110 (2006)
75. Artemiev A N et al. *Proc. SPIE* **5539** 208 (2004)
76. Artemiev A N et al. *Crystallogr. Rep.* **49** (Suppl.) S166 (2004)
77. Potlovskii K G et al. *Izv. Ross. Akad. Nauk, Ser. Fiz.* **68** (4) 477 (2004) [*Bull. Russ. Acad. Sci., Phys.* **68** 539 (2004)]
78. Tomie T, Japan Patent No. 6-045288(1994); USA Patent No. 5,594,773 (1997)
79. Protopopov V V et al. "Issledovanie vozmozhnosti sozdaniya sostavnoi rentgenovskoi linzy" ("Feasibility investigation of a compound X-ray lens"), Preprint No. 20 (St.-Petersburg: FTI RAN, 1997)
80. Snigirev A A et al. *Proc. SPIE* **3151** 164 (1997)
81. Elleaume P *Nucl. Instrum. Meth. Phys. Res. A* **412** 483 (1998)
82. Elleaume P *J. Synchrotron Rad.* **5** 1 (1998)
83. Snigirev A et al. *Appl. Opt.* **37** 653 (1998)
84. Baron A Q R et al. *Appl. Phys. Lett.* **74** 1492 (1999)
85. Cremer J T et al. *Rev. Sci. Instrum.* **70** 3545 (1999)
86. Nygren D R et al., USA Patent No. 6,091,798 (1999)
87. Lengeler B et al. *J. Synchrotron Rad.* **6** 1153 (1999)
88. Lengeler B et al. *J. Appl. Phys.* **84** 5855 (1998)
89. Castelnau O et al. *Nucl. Instrum. Meth. Phys. Res. A* **467–468** 1245 (2001)
90. Lengeler B et al. *Appl. Phys. Lett.* **74** 3924 (1999)
91. Baron A Q R et al. *J. Synchrotron Rad.* **6** 953 (1999)

92. Kohmura Y et al. *Rev. Sci. Instrum.* **70** 4161 (1999)
93. Dudchik Yu I, Kolchevsky N N *Nucl. Instrum. Meth. Phys. Res. A* **421** 361 (1999)
94. Aristov V et al. *Nucl. Instrum. Meth. Phys. Res. A* **470** 131 (2001)
95. Grigoriev M et al. *Proc. SPIE* **4501** 185 (2001)
96. Nazmov V et al. *Galvanotekhnik* (*Mikrosystemtechnik*) **4** 964 (2006)
97. Nazmov V et al., in *Digest Report XVI Intern. Synchrotron Radiation Conf.* (*SR2006*) p. 135
98. Snigireva I A et al. *Proc. SPIE* **5539** 20 (2004)
99. Kuyumchyan A V et al. *Poverkhnost': Rentgen., Sinkhrotron., Neitron. Issled.* (6) 29 (2006)
100. Shastri S D et al. *Opt. Commun.* **197** 9 (2001)
101. Snigirev A et al., in *Coll. Abstracts of 8th Biennial Conf. on High Resolution X-Ray Diffraction and Imaging* (*XTOP-2006*)*, Germany, 19–22 September 2006*, p. 200
102. Grigor'ev M V et al., in *Nanofizika i Nanoelektronika*: *Mezhdunar. Simpozium, 10–14 Marta 2007 g., Nizhnii Novgorod* (Nanophysics and Nanoelectronics: XI Intern. Symp., 10–14 March 2007, Nizhnii Novgorod) Vol. 2 (N. Novgorod: Institute for the Physics of Microstructures, Russian Academy of Sciences, 2007) p. 339
103. Snigirev A A et al. *Proc. SPIE* **4783** 1 (2002)
104. Protopopov V V, Valiev K A *Opt. Commun.* **151** 297 (1998)
105. Kohn V, Snigireva I, Snigirev A *Opt. Commun.* **216** 247 (2003)
106. Kohn V G *Zh. Eksp. Teor. Fiz.* **124** 224 (2003) [*JETP* **97** 204 (2003)]
107. Kohn V et al. *J. Phys. IV* (France) **104** 217 (2003)
108. Kohn V G, Snigireva I, Snigirev A *Poverkhnost': Rentgen., Sinkhrotron., Neitron. Issled.* (1) 33 (2003)
109. Kohn V G *Izv. Ross. Akad. Nauk, Ser. Fiz.* **68** 468 (2004) [*Bull. Russ. Acad. Sci., Phys.* **68** 529 (2004)]
110. Snigireva I A, Kohn V G, Snigirev A A *Proc. SPIE* **5539** 218 (2004)
111. Kohn V G *Kristallografiya* **51** 605 (2006) [*Crystallogr. Rep.* **51** 564 (2006)]
112. Shabel'nikov L G "Method of fabricating X-ray refractive lenses with a profile of revolution", Russian Federation Patent No. 280204 (publ. 20.04.2007, appl. 10.10.2003)
113. Shabel'nikov L G, Fel'dman E V, Rudavets M G *Poverkhnost': Rentgen., Sinkhrotron., Neitron. Issled.* (1) 46 (2002)
114. Aristov V V et al. "Method of fabricating X-ray refractive lenses", Russian Federation Patent No. 2298852 (publ. 10.05.2007, appl. 14.10.2005)
115. Snigireva I et al. *Nucl. Instrum. Meth. Phys. Res. A* **467–468** 982 (2001)
116. Snigireva I et al. *Proc. SPIE* **4499** 64 (2001)
117. Shabel'nikov L G, Aristov V V, in *Nanofizika i Nanoelektronika*: *X Mezhdunar. Simpozium, 13–17 Marta 2006 g., Nizhnii Novgorod* (Nanophysics and Nanoelectronics: X Intern. Symp., 13–17 March 2006, Nizhnii Novgorod) (N. Novgorod: Institute for the Physics of Microstructures, Russian Academy of Sciences, 2006) p. 406
118. Aristov V V, Shabel'nikov L G *Defektoskopiya* (8) 60 (1988)
119. Aristov V V, Chukhovskii F N, Shabel'nikov L G *Kristallografiya* **34** (6) 1365 (1989) [*Sov. Phys. Crystallogr.* **34** 822 (1989)]
120. Nazmov V et al. *Nucl. Instrum. Meth. Phys. Res. B* **217** 409 (2004)
121. Naz'mov V P et al. *Izv. Ross. Akad. Nauk, Ser. Fiz.* **68** 482 (2004) [*Bull. Russ. Acad. Sci., Phys.* **68** 544 (2004)]
122. Shabel'nikov L G, in *Digest Report XVI Intern. Synchrotron Radiation Conf.* (SR2006) p. 129
123. Aristov V V et al. *Poverkhnost': Rentgen., Sinkhrotron., Neitron. Issled.* (1) 89 (2001)
124. Cavalleri A et al. *Opt. Photon. News* (5) 29 (2001)
125. Tur'yanskii A G, Pirshin I V, in *Rentgenovskaya Optika-2004*: *Materialy Soveshchaniya, Nizhnii Novgorod, 2–6 Maya 2004 g.* (X-Ray Optics-2004: Conf. Proc., Nizhnii Novgorod, 2–6 May 2004) (N. Novgorod: Institute for the Physics of Microstructures, Russian Academy of Sciences, 2004) p. 237
126. Snigireva I, Kohn V, Snigirev A *Nucl. Instrum. Meth. Phys. Res. A* **467–468** 925 (2001)
127. Shabel'nikov L G et al. *Poverkhnost': Rentgen., Sinkhrotron., Neitron. Issled.* (1) 41 (2002)
128. Shabel'nikov L G et al., in *Rentgenovskaya Optika-2002*: *Materialy Soveshch., 18–21 Marta 2002 g., Nizhnii Novgorod* (X-Ray Optics-2002: Conf. Proc., Nizhnii Novgorod, 18–21 March 2002) (N. Novgorod: Institute for the Physics of Microstructures, Russian Academy of Sciences, 2002) p. 80
129. Shabel'nikov L et al. *Proc. SPIE* **4783** 55 (2002)
130. Arms D A et al. *Rev. Sci. Instrum.* **73** 1492 (2002)
131. Cremer J T et al. *Rev. Sci. Instrum.* **74** 2262 (2003)
132. Dufresne E M et al. *Appl. Phys. Lett.* **79** 4085 (2001)
133. Jark W et al. *Appl. Phys. Lett.* **78** 1192 (2001)
134. Bongaerts J H H et al. *J. Synchrotron Rad.* **9** 383 (2002)
135. The HORIBA X-ray guide tube technology, http://www.jobinyvon.com/usadivisions/XRay/xgt5000_probe.htm
136. UNISANTIS®, http://www.unisantis.com/
137. Simionovici A S et al. *Proc. SPIE* **5535** 232 (2004)
138. Bleuet P et al., in *Coll. Abstracts of 8th Biennial Conf. on High Resolution X-Ray Diffraction and Imaging* (*XTOP-2006*)*, Germany, 19–22 September 2006,* TO8-1
139. Simionovici A et al. *IEEE Trans. Nucl. Sci.* **47** 2736 (2000)
140. Chukalina M V et al., in *Nanofizika i Nanoelektronika*: *X Mezhdunar. Simpozium, 13–17 Marta 2006 g., Nizhnii Novgorod* (Nanophysics and Nanoelectronics: X Intern. Symp., 13–17 March 2006, Nizhnii Novgorod) (N. Novgorod: Institute for the Physics of Microstructures, Russian Academy of Sciences, 2006) p. 412
141. Chumakov A I et al. *Appl. Phys. Lett.* **77** 31 (2000)
142. Chumakov A I et al. *Poverkhnost': Rentgen., Sinkhrotron., Neitron. Issled.* (1) 38 (2001)
143. Ungár T et al. *Acta Mater.* **55** 1117 (2007)
144. Drakopoulos M et al. *J. Phys. D*: *Appl. Phys.* **36** A214 (2003)
145. Schmahl G, Rudolph D (Eds) *X-Ray Microscopy*: *Proc. of the Intern. Symp., Göttingen, FRG, September 14–16, 1983* (Berlin: Springer-Verlag, 1984) [Translated into Russian (Moscow: Mir, 1987)]
146. Artyukov I A et al., in *Rentgenovskaya Optika-2004*: *Materialy Soveshchaniya, Nizhnii Novgorod, 2–6 Maya 2004 g.* (X-Ray Optics-2004: Conf. Proc., Nizhnii Novgorod, 2–6 May 2004) (N. Novgorod: Institute for the Physics of Microstructures, Russian Academy of Sciences, 2004) p. 98
147. Tikhonov A N, Arsenin V Ya, Timonov A A *Matematicheskie Zadachi Komp'yuternoi Tomografii* (Mathematical Problems of Computer Tomography) (Moscow: Nauka, 1987)
148. Natterer F *The Mathematics of Computerized Tomography* (Chichester: Wiley, 1986) [Translated into Russian (Moscow: Mir, 1990)]
149. Reznikova E et al., in *Coll. Abstracts of 8th Biennial Conf. on High Resolution X-Ray Diffraction and Imaging* (*XTOP-2006*)*, Germany, 19–22 September 2006*, p. 198
150. Andreev A V et al., in *Trudy XVI Mezhdunar. Konf. po Ispol'zovaniyu Sinkhrotronnogo Izlucheniya, 10–15 Iyulya 2006 g., Novosibirsk, Rossiya* (Proc. XVI Intern. Synchrotron Radiation Conf., SR-2006, 10–15 July 2006, Novosibirsk, Russia) (Novosibirsk: IYaF SO RAN, 2006) p. 132
151. SKYSCAN, http://www.skyscan.be
152. Birner A et al. *Adv. Mater.* **13** 377 (2001)
153. Benisty H et al. *Appl. Surf. Sci.* **164** 205 (2000)
154. Aristov V V et al. *Mikrosistemnaya Tekhnika* (9) 37 (2001)
155. Starkov V V *Laser Phys.* **14** 664 (2004)
156. Starkov V V *Phys. Status Solidi A* **197** 22 (2003)
157. Drakopoulos M et al. *Appl. Phys. Lett.* **86** 014102 (2005)
158. Malaguti G et al. *Proc. SPIE* **5900** 159 (2005)
159. Vadawale S V et al. *Proc. SPIE* **5900** 338 (2005)
160. Gubarev M, Chery A, Brian R *Proc. SPIE* **5900** 232 (2005)
161. Kitamoto S *Proc. SPIE* **5900** 377 (2005)
162. Tsunemi H et al. *Proc. SPIE* **5900** 184 (2005)
163. Shibata R et al. *Proc. SPIE* **5900** 205 (2005)
164. Koglin J E et al. *Proc. SPIE* **5900** 266 (2005)
165. Gorenstein P, Phillips J D, Reasenberg R D *Proc. SPIE* **5900** 369 (2005)
166. Squillante M R et al. *Proc. SPIE* **5923** 188 (2005)
167. Reid P B, Glenn P, Bookbinder J *Proc. SPIE* **5900** 137 (2005)
168. Arenberg J W, Lay C, Lo A *Proc. SPIE* **5900** 405 (2005)